Holographic duality between bulk topological order and boundary mixed-state order

Tsung-Cheng Lu,^{1,*} Yu-Jie Liu,^{2,†} Sarang Gopalakrishnan,^{3,‡} and Yizhi You^{4,§} ¹ Joint Center for Quantum Information and Computer Science, University of Maryland, College Park, Maryland 20742, USA ²Center for Theoretical Physics - a Leinweber Institute, Massachusetts Institute of Technology, Cambridge, MA 02139, USA ³Department of Electrical and Computer Engineering, Princeton University, Princeton, NJ 08544, USA ⁴Department of Physics, Northeastern University, Boston, MA, 02115, USA (Dated: November 26, 2025)

We introduce a holographic framework for analyzing the steady states of repeated quantum channels with strong symmetries. Using channel-state duality, we show that the steady state of a d-dimensional quantum channel is holographically mapped to the boundary reduced density matrix of a (d+1)-dimensional wavefunction generated by a sequential unitary circuit. From this perspective, strong-to-weak spontaneous symmetry breaking (SWSSB) in the steady state arises from the anyon condensation on the boundary of a topological order in one higher dimension. The conditional mutual information (CMI) associated with SWSSB is then inherited from the bulk topological entanglement entropy. We make this duality explicit using isometric tensor network states (isoTNS) by identifying the channel's time evolution with the transfer matrix of a higher-dimensional isoTNS. Built on isoTNS, we further construct continuously tunable quantum channels that exhibit distinct mixed-state phases and transitions in the steady states.

CONTENTS		A. 2d 0-form SW-SSB	13
		B. 2d 1-form SW-SSB	14
I. Introduction	1	C. 2d subsystem SW-SSB	15
		D. 1d fermion parity SW-SSB	16
II. Basic framework and setup	3	E. 2d fermionic 1-form SW-SSB	16
A. Brief review of SW-SSB	3	F. SW-SSB from non-CPTP maps	17
B. Holographic perspective for quantum		2. 6. 6. 6. 6. 6. 6. 6. 6. 6. 6. 6. 6. 6.	
channels	3	VI. Outlook	18
C. Strongly symmetric channel and SW-SSB			
from holography	4	Acknowledgments	19
III. 1d SW-SSB as the boundary of 2d topological		A. Derivation of the deformed toric code	19
order	5		
A. Holographic description via sequential		B. Absence of finite- g transition	20
circuits	5		
B. Bulk-boundary correspondence from	_	C. Emergence of SW-SSB at finite depth	20
generalized symmetries	7		
C. Conditional mutual information	8	D. Holographic bulk of the 2d 0-form SW-SSB	21
D. Fidelity correlator	8		
E. Necessity of infinite-depth for SW-SSB in 1d	9	E. Holographic bulk of the 2d 1-form SW-SSB	22
IV. Holographic duality from isoTNS	9	E. Helemanhie halls of the 2d formionic 1 forms	
A. Forced nontrivialness of isoTNS from	5	F. Holographic bulk of the 2d fermionic 1-form SW-SSB	23
channel-state duality	10	2 M-22D	23
B. Continuously-tuned quantum channels and	10	References	23
U(1) SW-SSB critical point	11	Telefology	20
r () 8			
V. General discussion for SW-SSB under		I. INTRODUCTION	
holographic duality	13	1. 11/11/00/00/11/01/	

The classification of many-body states into equivalence classes, called phases of matter, is a central task in manybody physics [1]. Informally, a phase of matter is a set of states that share the same universal long-distance properties: for example, long-range magnetic order, superfluidity, or topological order. The notion of phases has been

^{*} tclu@umd.edu

[†] yujieliu@mit.edu

[‡] sgopalakrishnan@princeton.edu

[§] v.you@northeastern.edu

made precise in the context of ground states of gapped local Hamiltonians: two such states are in the same phase if there exists a finite-time quasilocal evolution that transforms one into the other [2–5].

More generally, for equilibrium ordered phases-namely, those that spontaneously break global symmetries-there is a universal description based on Landau theory. Neither framework generalizes to a family of states that are increasingly relevant to present-day quantum devices: namely, mixed states that arise from nonequilibrium processes such as noise, measurements, and error correction. The toric code subject to noise is a canonical example of a model with distinct mixed-state phases: below a certain threshold, the code retains logical information, which can be perfectly retrieved in the thermodynamic limit by error correction; above threshold, the logical information is irretrievable [6, 7]. The state of the toric code subject to sub-threshold noise levels does not appear to be a thermal state of any local Hamiltonian; its residual topological order is not captured by any conventional correlation function. Nevertheless, it is a sharply distinct phase from the trivial one. In the past few years, many other examples of mixed-state phases and phase transitions have been found [8–62], further motivating the quest for a definition of "mixed-state phases" that formally captures these distinctions.

In the context of equilibrium pure-state phases, symmetry plays a key part in the classification. Even phases that were initially described as lying outside a symmetrybased classification, such as a large class of topologically ordered phases, are now understood in terms of higherform symmetries [63]. In mixed states, these symmetries can come in two varieties, "strong" or "weak": intuitively, strongly symmetric mixed states have a definite eigenvalue of the symmetry charge, while weakly symmetric states can be mixtures (but not superpositions) of charge sectors. (We will define these concepts more precisely in Sec.II.) A state can spontaneously break either a strong or a weak symmetry to nothing: this would be conventional spontaneous symmetry breaking, which can be detected by conventional correlators. However, it can also exhibit the intrinsically mixed-state phenomenon of spontaneous strong-to-weak symmetry breaking (SW-SSB) [53–58]. An intuitive example of SW-SSB occurs in the maximally mixed state with a definite symmetry charge (for simplicity, consider a simple U(1) charge). This state is akin to a thermal state in the canonical ensemble that has no form of conventional order. However, if one loses information about part of the system, this information cannot be reconstructed locally, since any local reconstruction would not "know about" the global charge of the system. Thus, a mixed state with SW-SSB marks a distinct phase of matter from, for example, a single bit string, which can be reconstructed locally. Although this example is simple and classical, SW-SSB is a general framework that can capture a huge variety of distinct mixed-state phases and phase transitions, including error correction transitions [54–58, 60, 64–69].

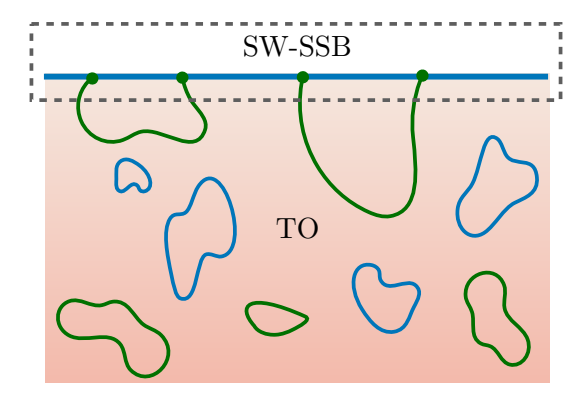


FIG. 1. Holographic correspondence between an SW-SSB mixed state in d dimensions and a topological order in d+1 dimensions. In a \mathbb{Z}_2 topological order, the two loop-like symmetries in the bulk can be pushed to the 1d boundary, where they manifest as a strong symmetry and a weak symmetry. The mutual anomaly between these symmetries signals an SW-SSB in the boundary reduced density matrix.

So far, much work on mixed-state phases and SW-SSB has focused on transitions that occur in finite-time dynamics, e.g., the toric code subject to noise for a finite time. However, the most natural object to study in a general nonequilibrium process is its late time steady state density matrix [52, 61, 65, 66, 70, 71]. The classification of steady states of Lindblad master equations was recently explored using principles analogous to those for general mixed states [72]; whether all mixed states can be realized as steady states of Lindblad master equations, however, remains an open question. Steady states are more structured than generic mixed states because they have a holographic representation in one higher dimension: they correspond to the boundary states of sequential quantum circuits [46, 73, 74] (or equivalently, isometric tensor networks [75]). Physically, this correspondence can be understood as follows. A Markov process consists of a system repeatedly interacting with its environment. This repeated interaction generates a pure state in a spacetime "bulk" consisting of the system plus its environments at every time step. From this pure state, the system's steady state (which lives on the top spacetime "boundary") can be reached by tracing out the environment qubits that form the spacetime bulk. The question we address in this work is: what kind of spacetime bulk gives rise to SW-SSB in the steady state? Our main result can be summarized as follows: we argue (and give explicit constructions demonstrating) that the spacetime bulk could be topologically ordered, and that the SW-SSB boundary arises from boundary condensation of anyons of the bulk topological order; see Fig.1. We discuss this correspondence between bulk topological order and boundary mixed-state SW-SSB in a variety of settings.

The rest of this work is organized as follows. In Sec.II, we review the main concepts of SW-SSB and present the holographic framework that relates a steady state to a

higher-dimensional holographic wavefunction via channel/state duality. Sec.III provides a detailed discussion of the holographic correspondence between 1d SW-SSB and 2d topological order through a concrete example. In Sec.IV, we reformulate the holographic duality using the isoTNS (isometric tensor network state) formalism, and discuss its applications. Sec.V extends the discussion to various generalized symmetries—including higher-form, subsystem, and fermionic symmetries. Finally, in Sec.VI, we conclude by highlighting open questions and future directions.

II. BASIC FRAMEWORK AND SETUP

In this section, we will first briefly review the concept of strong-to-weak spontaneous symmetry breaking (SW-SSB) in many-body mixed states [54–56], and then show how they can be naturally understood via a holographic perspective.

A. Brief review of SW-SSB

In a mixed quantum state ρ , a symmetry U can have two different manifestations, i.e., strong or weak. The strong symmetry refers to the property that $U\rho \propto \rho$. in which case all the pure states in any ensemble decomposition carry the same symmetry charges. On the other hand, the weak symmetry only requires $U\rho U^{\dagger} = \rho$, so that pure states in the mixed-state ensemble are allowed to carry distinct charges. Due to these two different notions of symmetries, mixed states may exhibit a new pattern of symmetry breaking, where a strong symmetry can be spontaneously broken down to the weak one. Physically, this indicates the strongly symmetric mixed state does not have long-range order in charged operators, i.e. $\lim_{|i-j|\to\infty} \operatorname{Tr}(\rho O_i O_j) \to 0$, but still, it is possible to decompose the mixed state into an ensemble of long-range ordered state, namely, $\rho = \sum_n p_n |\psi_n\rangle \langle \psi_n|$, where $\lim_{|i-j|\to\infty} \langle \psi_n| O_i O_j |\psi_n\rangle \neq 0$ [18]. In particular, the 'averaged' long-range order in the ensemble can be diagnosed by the so-called fidelity correlator [56], defined as the fidelity between ρ and $O_i O_j \rho O_i^{\dagger} O_i^{\dagger}$:

$$F_{ij} = \text{Tr}\sqrt{\sqrt{\rho}O_iO_j\rho O_i^{\dagger}O_j^{\dagger}\sqrt{\rho}} \neq 0$$
 (1)

for $|i-j| \to \infty$. The presence of long-range order in the fidelity correlator further indicates that the resulting mixed state is not locally recoverable. In other words, the steady state features a divergent Markov length and non-vanishing conditional mutual information.

As a simple example, consider a 1d lattice with each qubit per site with a strong \mathbb{Z}_2 symmetry generated by $\prod_i X_i$, the maximally mixed state with strong \mathbb{Z}_2 symmetry

metry exhibits SW-SSB:

$$\rho \propto 1 + \prod_{i} X_{i}. \tag{2}$$

It is simple to see that $\text{Tr}(\rho Z_i Z_j) = 0 \quad \forall i \neq j$, so ρ does not have long-range order in local, linear observables. However, the fidelity correlator $F_{ij} = 1$, and correspondingly, ρ admits an ensemble of long-range order pure states

$$\rho \propto \sum_{z} |\psi_{z}\rangle \langle \psi_{z}|, \qquad (3)$$

where $|\psi_z\rangle \propto (1+\prod_i X_i)|z\rangle$, i.e., a cat state whose domain wall configuration is fixed by the Pauli-Z basis state $|z\rangle$.

Since SW-SSB only manifests the order in each pure state in the ensemble without showing any order in any linear observables in the density matrix, it is regarded as a novel phenomenon intrinsic to many-body mixed states. As such, there has been a surge of interest in understanding SW-SSB. Below, we will provide one novel perspective, showing that SW-SSB mixed states naturally admit a holographic description in terms of a wave function in one higher dimension.

B. Holographic perspective for quantum channels

Our holographic description of SW-SSB is based on the duality inspired by Ref.[76, 77]: the output of a repeated quantum channel in d spatial dimensions is exactly the boundary reduced density matrix of a (d+1)-dimensional wavefunction generated by sequential unitary circuits. This insight allows us to understand SW-SSB, which generically appears in the steady state of a repeated quantum channel, in terms of a wavefunction in one higher dimension. Here, we will introduce the duality framework for general quantum channels. The special class of channels that preserve strong symmetries and give rise to SW-SSB steady states will be discussed in Sec.II C.

Given the system qubits in d spatial dimensions, a local quantum channel can be implemented by entangling with the ancilla qubits (in d spatial dimensions as well) via a local unitary circuit U, followed by tracing out the ancilla qubits. Specifically, when the ancilla qubits are initialized as the product state $|0\rangle_a \equiv |000...\rangle$, tracing out the ancilla qubits after U implements a completely positive and trace-preserving (CPTP) quantum channel on the system qubits:

$$\mathcal{E}[\rho_0] = \operatorname{Tr}_a \left[U \left(\rho_0 \otimes |0\rangle \langle 0|_a \right) U^{\dagger} \right]$$
$$= \sum_m K_m \, \rho_0 \, K_m^{\dagger}. \tag{4}$$

where K_m defines the Kraus operator.

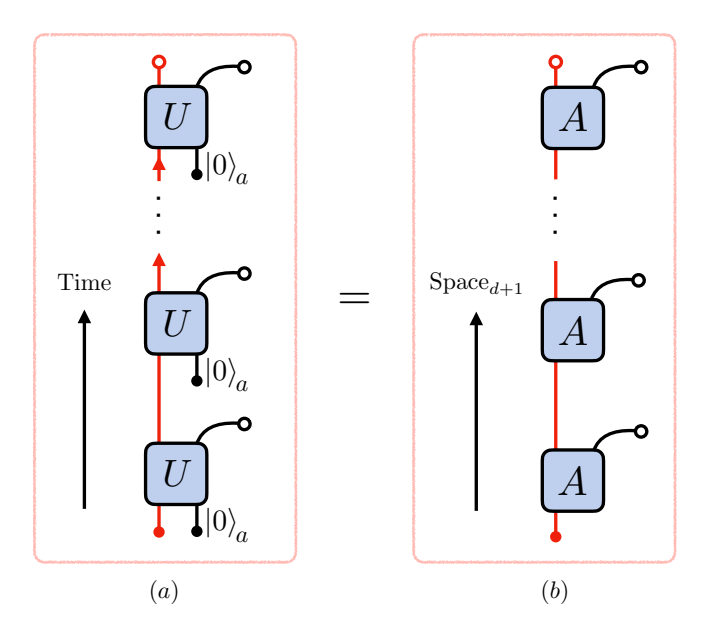


FIG. 2. (a) A repeated quantum channel acting on the system (wordline in red) in d spatial dimensions is equivalent to sequentially entangling the system with fresh ancilla qubits in various time slices, which generates a pure-state wavefunction in (d+1) spatial dimensions, as shown in (b). The system output under the repeated channel is the boundary reduced density matrix of this higher-dimensional wave function by tracing out the ancilla qubits.

When applying the quantum channel repeatedly, the system qubits are sequentially entangled with fresh d-dimensional ancilla qubits at various time slices, followed by tracing out all the ancilla qubits; see Fig.2(a). In particular, the arrangement of these ancilla qubits at various time slices introduces an extra spatial dimension, so that the repeated quantum channel defines a sequential unitary circuit, where the system qubits sequentially interact with ancilla qubits along this new spatial direction. The resulting circuit generates a wavefunction $|\Psi\rangle$ in (d+1) spatial dimensions, where the output of the system qubit lives on the boundary and the bulk is formed by the ancilla qubits; see Fig.2(b). Namely, the reduced density matrix on the boundary

$$\rho_s = \operatorname{Tr}_{\text{bulk}} \left[|\Psi\rangle\langle\Psi| \right]$$

is exactly the output of a repeated quantum channel. This holographic view of a steady state provides a new perspective for SW-SSB, as we will illustrate in the next subsection.

C. Strongly symmetric channel and SW-SSB from holography

To apply the holographic framework to SW-SSB, we consider a quantum channel \mathcal{E} with strong symmetry S, meaning that there is no exchange of symmetry charges

between the system and ancillae, and hence the charges within the system are conserved. In other words, if the input has the strong symmetry, i.e. $S\rho_0 \propto \rho_0$, the output of the channel will be strongly symmetric as well: $S\mathcal{E}[\rho_0] \propto \mathcal{E}[\rho_0]$. Mathematically, such a strongly symmetric channel demands that all Kraus operators commute with the symmetry operator $[K_m,S]=0$, or equivalently, in the dual sequential-circuit picture, the unitary gate U acting on the system and ancillae satisfies [U,S]=0, where we note that S only acts on the system.

A repeated quantum channel possessing a strong symmetry S will generically lead to a steady state that exhibits SW-SSB. Intuitively, this is because unstructured, repeated interactions with the environment tend to wash out any long-range order, leaving only the information associated with the global symmetry conservation law. In other words, the steady state is expected to be close to a maximally mixed state constrained by the strong symmetry (e.g., $\rho \sim 1 + \prod_i X_i$ in the case of a \mathbb{Z}_2 symmetry).

When the steady state of strongly symmetric channels exhibits SW-SSB, we can then adopt the framework in Sec.IIB to develop a holographic description with a wave function in one higher spatial dimension. This raises a central question: are the universal features of SW-SSB—such as the strong—weak symmetry anomaly, the non-vanishing conditional mutual information and fidelity correlator—holographically encoded in the higher-dimensional wave function?

To make the holographic duality explicit, we recast channel dynamics in a unifying isometric tensor-network state (isoTNS) representation [75]. IsoTNS are an expressive subclass of tensor networks that capture many gapped ground states, including all the 2d string-net topological orders [78, 79]. Enforcing isometry makes the transfer matrix of a (d+1)-dimensional isoTNS naturally dual to the time evolution of local quantum channels in d dimensions, where one of the spatial directions in the isoTNS can be viewed as a temporal direction in the channel dynamics; the dominant eigenvector of this transfer matrix yields the steady state. Thus, the steady state of any repeated quantum channel is the boundary reduced density matrix of a higher-dimensional isoTNS, with boundary degrees of freedom identified with the network's virtual bonds. The detailed discussion for SW-SSB based on the isoTNS framework will be presented in Sec.IV.

As we will elucidate in Sec.III and summarize in Table I, SW-SSB of a \mathbb{Z}_2 symmetry in 1d maps to the boundary reduced density matrix of a 2d \mathbb{Z}_2 topological order with a charge-condensed boundary. Notably, the strong symmetry condition maps to a virtual symmetry of the tensors, indicating that the higher-dimensional wavefunction carries a 1-form flux-loop symmetry. Likewise, the fidelity correlator that diagnoses

1d steady state of a channel	2d topological order
Strong symmetry	1-form symmetry generated by m-flux loop
Weak 1-form symmetry	1-form symmetry generated by e-charge loop
Strong to weak symmetry breaking	charge condensation on the boundary
Time evolution of quantum channel	Transfer matrix of isoTNS
Conditional mutual information	Topological entanglement entropy

TABLE I. A summary of the holographic duality discussed in Sec.III

SW-SSB arises from the 1-form charge-loop symmetry, whose open strings can terminate on the boundary [80–82]. Finally, the nonvanishing conditional mutual information in the boundary reduced density matrix, which signals SW-SSB, is holographically dual to the bulk topological entanglement entropy [83, 84].

III. 1D SW-SSB AS THE BOUNDARY OF 2D TOPOLOGICAL ORDER

With the basic formalism established in Sec. II, in this section, we will focus on a particular channel that gives rise to an SW-SSB steady state, and discuss the emergence of topological orders in one higher dimension.

Consider a 1d lattice with each qubit per site and a strong \mathbb{Z}_2 symmetry generated by $\prod_i X_i$, we are interested in the SW-SSB mixed state defined in Eq.2:

$$\rho \propto 1 + \prod_{i} X_{i},\tag{5}$$

To obtain such a mixed state from any pure state $|\psi\rangle$ with the strong \mathbb{Z}_2 symmetry, we consider the channel $\mathcal{E} = \prod_i \mathcal{E}_i^z \mathcal{E}_i^x$, with

$$\mathcal{E}_{i}^{z}[\rho_{0}] = (1 - p_{z})\rho_{0} + p_{z}Z_{i}Z_{i+1}\rho_{0}Z_{i}Z_{i+1},
\mathcal{E}_{i}^{x}[\rho_{0}] = (1 - p_{x})\rho_{0} + p_{x}X_{i}\rho_{0}X_{i},$$
(6)

The X-type noise renders the steady state an incoherent mixture of product states in the X basis, while the Z-type noise enforces equal weights among these X-basis product states. Therefore, for any $p_x, p_z > 0$, the repeated application of these two noise channels drives the system to the steady state (Eq.5)

$$\rho = \lim_{N \to \infty} \mathcal{E}^N[|\psi\rangle \langle \psi|],\tag{7}$$

which exhibits SW-SSB.

A. Holographic description via sequential circuits

To develop a holographic description, we observe that the 1d noise channel $(\mathcal{E} = \prod_i \mathcal{E}_i^z \mathcal{E}_i^x)$ can be obtained by

entangling system qubits with ancilla qubits on a 1d geometry, followed by tracing out the ancilla qubits. Therefore, the repeated application of the 1d channel, when including both system and ancilla qubits as a whole, can be understood as a sequential unitary circuit where the system qubits propagate and sequentially interact with the ancilla qubits that are arranged on a 2d lattice (Fig.3). In the language of tensor network formalism, the system qubits live in the bond space and the ancilla qubits live in the physical legs of a tensor network. Notably, as we will now show, the sequential circuit that induces the SW-SSB on the system qubits in fact prepares a 2d topological order of those ancilla qubits, thereby establishing an intriguing connection between SW-SSB and the topological order in one higher spatial dimension.

To establish the correspondence, we first discuss the sequential circuit that implements the noise channel in Eq.6.

ZZ channel: to realize the ZZ noise channel acting on two system qubits (say labeled by 1 and 2), we can first initialize an ancilla qubit (labeled by a) in the state $\sqrt{1-p_z} \mid + \rangle_a + \sqrt{p_z} \mid - \rangle_a$, so that the system qubits and the ancilla qubit together is described by

$$|\psi\rangle\left(\sqrt{1-p_z}\,|+\rangle_a + \sqrt{p_z}\,|-\rangle_a\right),$$
 (8)

where $|\psi\rangle$ denotes the state of the system qubits.

Now we apply the controlled gate $u_{zz} = (|+\rangle \langle +|)_a + (|-\rangle \langle -|)_a Z_1 Z_2$, resulting in the state

$$|\psi_{p_z}\rangle = \sqrt{1 - p_z} |\psi\rangle |+\rangle_a + \sqrt{p_z} Z_1 Z_2 |\psi\rangle |-\rangle_a.$$
 (9)

Tracing out the ancilla qubit a then realizes the desired Z-type noise channel (Eq.6) on the system qubits, where Z_1Z_2 is applied with probability p_z .

We note that when $p_z = \frac{1}{2}$, i.e. maximal decoherence, the ancilla qubit is initialized at $|0\rangle_a$, which is stabilized by Z_a , and the subsequent application of u_{zz} generates $Z_1Z_aZ_2$ stabilizer with eigenvalue +1. Away from $p_z = \frac{1}{2}$, the ancilla qubit is initialized at $\sqrt{1-p_z} |+\rangle_a + \sqrt{p_z} |-\rangle_a$, which can also be written as

$$e^{g_z X_a} |0\rangle \propto e^{g_z} |+\rangle + e^{-g_z} |-\rangle,$$
 (10)

with

$$e^{2g_z} = \frac{1 - p_z}{p_z}. (11)$$

Since the imaginary time evolution by $e^{g_z X_a}$ commutes with the controlled gate u_{zz} , the pure state $|\psi_{p_z}\rangle$ (describing both the system qubits and ancilla qubits) for general p_z can be obtained by applying an imaginary time evolution on the pure state at $p_z = \frac{1}{2}$, in which case the ancilla qubit is initialized at $|0\rangle$:

$$|\psi_{p_z}\rangle \propto e^{e^{g_z X_a}} |\psi_{p_z = \frac{1}{2}}\rangle$$
 (12)

This relation will be useful when we investigate the state of the ancilla qubits later.

X channel: to realize the X noise channel acting on a system qubit (labeled by s), we can first initialize an ancilla qubit (labeled by a) in the state $\sqrt{1-p_x}\,|0\rangle_a+\sqrt{p_x}\,|1\rangle_a$, so that the state is given by

$$|\psi\rangle\left(\sqrt{1-p_x}\left|0\right\rangle_a + \sqrt{p_x}\left|1\right\rangle_a\right).$$
 (13)

Now we apply the controlled gate $(|0\rangle \langle 0|)_a + (|1\rangle \langle 1|)_a X_s$, resulting in the state

$$|\psi_{p_x}\rangle = \sqrt{1 - p_x} |\psi\rangle |0\rangle_a + \sqrt{p_x} X_s |\psi\rangle |1\rangle_a.$$
 (14)

Tracing out the ancilla qubit a then realizes the desired X-noise channel on the system qubits, where X_s is applied with probability p_x .

At $p_x = \frac{1}{2}$, i.e. maximal decoherence, the ancilla qubit is initialized at $|+\rangle_a$. Away from $p_x = \frac{1}{2}$, the ancilla qubit is initialized at $\sqrt{1-p_x} |0\rangle_a + \sqrt{p_x} |1\rangle_a$, which can also be written as

$$e^{g_x Z_a} \left| + \right\rangle \propto e^{g_x} \left| 0 \right\rangle + e^{-g_x} \left| 1 \right\rangle,$$
 (15)

with

$$e^{2g_x} = \frac{1 - p_x}{p_x}. (16)$$

Therefore, the pure state $|\psi_{p_x}\rangle$ for general p_x can be obtained by an imaginary time evolution acting on the pure state at $p_x = \frac{1}{2}$, in which case, the ancilla qubit is initialized at $|+\rangle$:

$$|\psi_{p_x}\rangle \propto e^{e^{g_x Z_a}} |\psi_{p_x = \frac{1}{2}}\rangle$$
 (17)

Repeated quantum channel: with the above ingredients, one can consider a 2d lattice with each ancilla qubit per link: the ancilla qubits on the horizontal (x) links and vertical (y) links are responsible for the ZZ channels and X channels, respectively. The repeated quantum channel can then be understood as a process where the system qubits on 1d move upward to sequentially interact with these ancilla qubits row by row (Fig.3). The output of the system qubits under the repeated quantum channel lives on the top boundary of the 2d lattice, which can be obtained by tracing out the

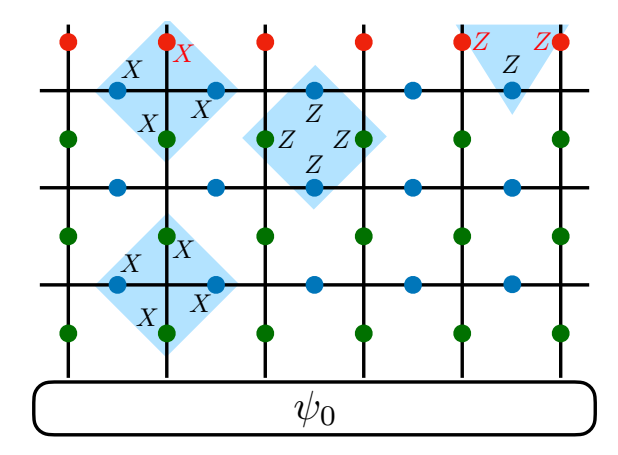


FIG. 3. A repeated quantum channel can be viewed as a sequential unitary circuit where a 1d system initialized at $|\psi_0\rangle$ propagates upward and sequentially interacts row by row with ancilla qubits (shown in green and blue). Tracing out the green and blue qubits implements the X and ZZ noise channels, respectively. The reduced density matrix on the 1d top boundary (colored in red) represents the output of the repeated quantum channel. At $p_z = p_x = \frac{1}{2}$, the bulk has the fixed-point toric-code topological order, and the top boundary is the SW-SSB state, i.e. $\propto (1 + \prod_i X_i)$.

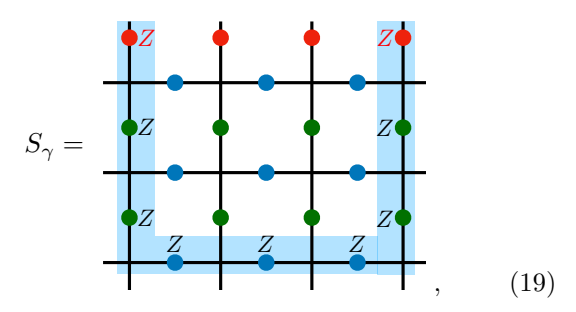
ancilla qubits. Notably, without tracing out the ancilla qubits, the pure state generated by the sequential circuit is a deformed toric-code wave function (See Appendix.A for derivation):

$$|\Psi^{2d}(g_x, g_z)\rangle = \prod_{\ell \in x \text{ link}} e^{g_z X_\ell} \prod_{\ell \in y \text{ link}} e^{g_x Z_\ell} |\text{TC}\rangle, \quad (18)$$

where the deformation strengths g_z and g_x are fixed by the noise rates p_z and p_x via Eq.11 and Eq.16.

The maximal decoherence, i.e. $p_x = p_z = \frac{1}{2}$, corresponds to vanishing string tensions $g_z = g_x = 0$, leading to the fixed-point toric code, whose top 1d boundary exhibits a SW-SSB. Notably, the bulk toric-code topological order vanishes only when $g_z = \infty$ or $g_x = \infty$. This can be checked by computing the wavefunction overlap $\langle \Psi^{2d}(g_x, g_z) | \Psi^{2d}(g_x, g_z) \rangle$, which is only singular when sending g_z or g_x to infinity (see Appendix.B). Heuristically, the factor $e^{g_z X_\ell}$ on an x-link tends to create pairs of m-fluxes that are constrained to move only along the y direction. Likewise, the factor $e^{g_x Z_\ell}$ on the y-link creates pairs of e-charges whose motion is restricted to the y direction as well. Such spatial anisotropy does not favor the proliferation of either anyon species in the bulk; consequently, the system remains topologically ordered for finite deformation. This contrasts with the isotropic deformation $e^{g\sum_{\ell}Z_{\ell}}\left|\mathrm{TC}\right\rangle$ [85, 86], which allows for e-charge condensation at a finite q. In that case, the wavefunction overlap maps to the partition function of the 2d Ising model, whose finite-temperature transition corresponds to a finite q transition. In the holographic picture, the robustness of the topological order in our deformed toriccode wavefunction (Eq.18) implies that the 1d SW-SSB steady state persists for any nonzero p_z, p_x in the infinite-depth limit of the repeated channel.

We now discuss more details about the holographic wavefunction above. We will focus on the discussion on the fixed-point limit $g_x = g_z = 0$. All universal features will apply equally to the deformed toric code (with finite g_x, g_z) since they belong to the same topologically ordered phase. At $p_x = p_z = \frac{1}{2}$, as shown in Eq.18, the holographic wavefunction in 2d is a fixed-point toric code, with the stabilizers specified in Fig.3. In particular, since the 1d system acted by the repeated quantum channel is defined on a ring (namely, the periodic boundary condition), the toric code has the topology of a cylinder with periodic boundary conditions along the x (horizontal) direction and open boundaries along the y (vertical) direction. The bottom boundary and the top boundary are the input and output of the repeated quantum channel, respectively. In particular, the ZZZ type stabilizer (shown in the upper right of Fig.3), together with the $Z^{\otimes 4}$ stabilizer around any plaquette in the bulk, implies the existence of the following open string stabilizer:



where γ can be freely deformable. The physical meaning of this stabilizer can be understood as follows: an open Z string operator in the bulk is responsible for creating two e particles on the two vertices on the endpoints of the string. As such, S_{γ} can be imagined as a process in which a pair of e particles is dragged to the boundary and condenses. In other words, the top 1d edge is specified by the rough boundary condition, interpretable as an e-condensed boundary. The condensation of pairs of e charges on the boundary is essential since when tracing out the bulk, the symmetry operator S_{γ} of the 2d pure state becomes a weak symmetry of the reduced density matrix ρ on the top boundary:

$$Z_i Z_j \rho Z_i Z_j = \rho. \tag{20}$$

There is also a stabilizer $\prod_{i \in \text{top edge}} X_i$ on all the red qubits on the top boundary.

$$\prod_{i \in \text{top edge}} X_i |\Psi^{2d}(g_x, g_z)\rangle = |\Psi^{2d}(g_x, g_z)\rangle \qquad (21)$$

Note that this equation holds for any finite g_x, g_z . The existence of this global symmetry acting on the 1d line is due to the fact that the input state has a fixed Z_2 charge,

which is preserved throughout the channel dynamics. As such, when tracing out the bulk qubits, leaving on the red qubits, the corresponding reduced density matrix ρ (i.e., the steady state of the quantum channel) has $\prod_i X_i$ as a strong symmetry:

$$\prod_{i} X_{i} \rho = \rho. \tag{22}$$

Without tracing out the bulk qubits, this symmetry measures the global flux threading the cylinder and generates the 1-form symmetry associated with the m-loop, so that the toric-code topological order is defined on a fixed symmetry sector.

B. Bulk-boundary correspondence from generalized symmetries

SW-SSB of the state $\rho \propto \frac{1+\prod_i X_i}{2}$ can be understood as the mutual anomaly between a strong S symmetry and a weak G symmetry:

$$S: (\prod_{i} X_{i})\rho = \rho$$

$$G: (Z_{i}Z_{j})\rho(Z_{i}Z_{j}) = \rho.$$
(23)

Here we show that such a mutual anomaly can be traced back to the mutual anomaly between two strong 1-form symmetries in the bulk, a defining feature of a \mathbb{Z}_2 toric-code topological order.

A universal feature of the 2d \mathbb{Z}_2 topological order is a 1-form symmetry (associated with m-flux loops) and a 1-form symmetry (associated with e-charge loops), which together carry the 't Hooft anomaly. When defining on a cylinder, a contractible m-flux loop in the bulk can be deformed into a pair of non-contractible loops $W_{m,\text{bottom}}W_{m,\text{top}}$, with $W_{m,\text{top}}$ winding around the top boundary and $W_{m,\text{bottom}}$ winding around the bottom boundary. In particular, if the 2d topological order is an eigenstate of the m-loop operator on a cylinder, then $W_{m,\text{bottom}}$ and $W_{m,\text{top}}$ will individually carry a definite eigenvalue, so the boundary reduced density matrix exhibits the strong S symmetry.

Meanwhile, a 1-form e-charge loop in the bulk can be pushed to the top boundary, which becomes an open string operator terminating on the two points on the 1d boundary (see Eq.19). This open string operator remains a symmetry of the entire 2d pure state. It allows us to create a pair of charges, push them onto the edge, and condense them. Notably, when tracing out the bulk, this opening string symmetry of the 2d pure state reduces to the weak G symmetry on the 1d boundary.

Therefore, the mutual anomaly between a strong 0-form symmetry and a weak 1-form symmetry, which is responsible for the SW-SSB in 1d [21, 87–90], inherits

from the mutual anomaly between a strong 1-form symmetry and another strong 1-form symmetry, which are responsible for a 2d topological order.

Final remark: in Sec.III A, the higher-dimensional topological order emerges since we consider a repeated quantum channel, which can be thought of as a sequential unitary circuit to entangle the system qubits and ancilla gubits in one higher dimension. On the other hand, a generic wavefunction with a topological order may not be prepared by a sequential unitary circuit, so the exact mapping between the repeated quantum channel and the higher-dimensional quantum state no longer holds. Nevertheless, the symmetry-based perspective discussed in this subsection does not rely such a channel/state duality. In particular, any non-fixed point \mathbb{Z}_2 topological order always has two 1-form symmetries that can be emergent and acquire a finite dressing width [2, 88, 91]. This strongly suggests that the reduced density matrix supported near the boundary of the topological wavefunction generically exhibits SW-SSB. The necessary boundary thickness is set by the dressing length of the emergent 1-form symmetries. This hints at the robustness and generality of the holographic correspondence beyond the SW-SSB steady states generated by quantum channels; we further comment on this in Sec. III E.

C. Conditional mutual information

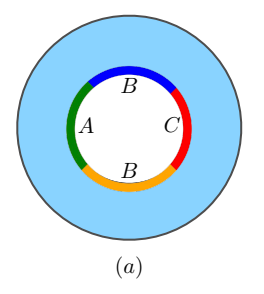
The holographic perspective also presents a unified framework for diagnosing SW-SSB and topological order based on certain information-theoretic quantities. Concretely, given an SW-SSB state on 1d, the conditional mutual information (CMI) between the two distant regions A and C conditioned on their complement B is non-vanishing [56](see Fig.4(a)):

$$I(A:C|B)$$

$$\equiv S(AB) + S(BC) - S(B) - S(ABC) > 0$$
(24)

As a sanity check, one may consider $\rho \propto 1 + \prod_i X_i$, and explicitly find $I(A:C|B) = \log 2$.

Physically, the non-vanishing CMI of the mixed state can be thought of as a consequence of the mutual anomaly between a 0-form strong symmetry and a 1-form weak symmetry [48]. In our holographic picture, such a mutual anomaly in the 1d system results from the mutual anomaly between two distinct types of strong 1-form symmetry of the 2d topologically ordered bulk, which implies a non-zero CMI (or equivalently, the topological entanglement entropy) under the partitioning shown in Fig.4(b) [48, 92, 93]. Therefore, the phenomenon of the non-vanishing CMI in the 1d SW-SSB and the non-vanishing CMI in 2d topological order, albeit defined via distinct partitioning, shares a common origin based on the symmetry perspective that finds a natural interpretation in our holographic duality.



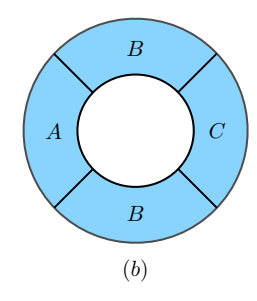


FIG. 4. (a) The inner circle and outer circle correspond to the top boundary and bottom boundary of a toric code defined on a cylinder. The reduced density matrix supported on the inner circle defines the 1d SW-SSB mixed state, which exhibits a non-zero conditional mutual information I(A,C|B). (b) The conventional setup for defining the CMI (or equivalently, the topological entanglement entropy) of the toric code state. The nonzero CMI in both (a) and (b) configurations arises from the mutual anomaly of the 1-form symmetries in the 2D toric code topological order.

D. Fidelity correlator

The fidelity correlator defined in Eq.1 provides a faithful diagnostic of SW-SSB:

$$F_{ij} = \text{Tr}\left[\sqrt{\sqrt{\rho}, O_i O_j \rho O_i O_j \sqrt{\rho}}\right]. \tag{25}$$

Here, O_i can be any charged operator localized at point i. For instance, when the global strong symmetry is $\prod_i X_i$, one may choose $O_i = Z_i$. Physically, F_{ij} detects the existence of a weak symmetry. This can be manifested by the fixed-point SW-SSB state $\rho \propto 1 + \prod_i X_i$, where the weak symmetry condition $Z_i Z_j \rho Z_i Z_j = \rho$ directly implies $F_{ij} = 1$. In particular, a long-range order in F_{ij} signals a divergent Markov length, implying that the mixed state is not locally recoverable and exhibits nonzero conditional mutual information [56].

Here we comment that a bulk 1-form charge symmetry that yields an e-condensed boundary provides a lower bound on the fidelity correlator. Suppose the repeated quantum channel admits a dual bulk wavefunction $|\Psi_{2d}\rangle$ whose boundary reduced density matrix is ρ . If the bulk has a 1-form symmetry with an e-condensed edge, there exists an open Wilson string operator W (e.g. the string operator in Eq.19) in the bulk that extends to and terminates at boundary points i,j, with a nonvanishing expectation value $\langle \Psi_{2d}|W|\Psi_{2d}\rangle = O(1)$. This Wilson string terminates on the edge at i,j, and its boundary endpoints are represented by operators O_i,O_j that—while not fixed microscopically—must be charged under the X 1-form symmetry.

Since $|\Psi_{2d}\rangle$ is a purification of the boundary density matrix ρ , the state $W|\Psi_{2d}\rangle$ is a purification of $O_iO_j\rho O_iO_j$. By Uhlmann's theorem [94], the fidelity between two density matrices equals the maximum overlap

over all of their purifications. Hence,

$$\langle \Psi_{2d} | W | \Psi_{2d} \rangle \le \text{Tr} \left[\sqrt{\sqrt{\rho}, O_i O_j \rho O_i O_j \sqrt{\rho}} \right],$$
 (26)

Therefore, the bulk Wilson-line expectation value $\langle \Psi_{2d}|W|\Psi_{2d}\rangle$ provides a lower bound for the fidelity correlator. As a corollary, for any bulk topological order that condenses the charge at its edge, its boundary reduced density matrix exhibits a nonvanishing fidelity correlator F_{ij} .

E. Necessity of infinite-depth for SW-SSB in 1d

In the previous discussion, we have focused mainly on the steady state of the channel defined in Eq.6, namely the mixed state $\rho \propto 1 + \prod_i X_i$ that exhibits SW-SSB. An important question is: what is the depth required for the output of the repeated quantum channel to exhibit SW-SSB with a non-zero fidelity correlator? Consider the symmetric input state $|+...\rangle$ as an example, under a single application of the ZZ channel, the output exhibits SW-SSB only when $p_z = \frac{1}{2}$, in which case the output is simply $\rho \propto 1 + \prod_i X_i$. For any $p_z < \frac{1}{2}$, in order to develop a non-vanishing fidelity correlator, the depth of the corresponding quantum channel needs to be infinite. While this has been known in the literature [55, 56] via a mapping to 1d classical statistical models, below we provide a heuristic argument for this phenomenon from a holographic perspective.

In our holographic duality framework, the depth of the repeated quantum channel is the size of the vertical (y) direction of the deformed toric-code wavefunction (Eq.18):

$$|\Psi^{2d}(g_x, g_z)\rangle = \prod_{\ell \in x \text{ link}} e^{g_z X_\ell} \prod_{\ell \in y \text{ link}} e^{g_x Z_\ell} |\text{TC}\rangle.$$
 (27)

At $p_z = \frac{1}{2}$, the holographic wavefunction is the fixed-point toric code, which has the deformable open Z string operator S_{γ} along any path γ (Eq.19; see also Fig.5 for the schematic), with two Pauli-Zs attached to the 1d top boundary. Such a symmetry operator for the pure-state wavefunction gives the weak symmetry for the 1d reduced density matrix, and leads to the non-decaying fidelity correlator.

For the deformed toric code, by expanding the exponential $\prod_{\ell \in x \text{ link}} e^{g_z X_\ell}$, one sees that it creates various Pauli-X insertions on horizontal (x) links of the toric code state. Since the string operator S_{γ} (Eq.19) can be deformed freely, its expectation will be modified only when the Pauli-X insertion form a string operator $W_{\tilde{\gamma}}$ that extends from the top boundary to the bottom boundary, in which case the intersection between γ and $\tilde{\gamma}$ cannot be avoided (shown in Fig.5). What is the probability of forming such an extended string $\tilde{\gamma}$? To provide a heuristic estimation, we can first write $e^{g_z X_\ell} \propto 1 + X_\ell \tanh g_z$,

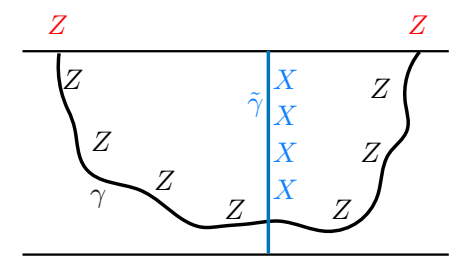


FIG. 5. The formation of the Pauli X string extending from the top boundary to the bottom boundary will modify the expectation value of S_{γ} string. Only when $L_{y} \to \infty$, the probability of such an X string will vanish, leading to the robustness of the S_{γ} string, and therefore, the emergence of SW-SSB on the top boundary.

so the probability amplitude for a single-X insertion is $\tanh q_z$. It follows that the weight for forming a string extending from the top to the bottom goes as $(\tanh g_z)^{L_y}$. On the other hand, the endpoint of the vertical string on the top boundary can occur at any position between i and j. Taking into account this multiplicity gives the probability weight $\sim |i-j|(\tanh g_z)^{L_y} = |i-j|(1-2p_z)^{L_y}$. For a large and fixed |i-j|, for any $0 < p_z < \frac{1}{2}$, the probability of the extended string will vanish only at $L_y \to \infty$. This provides a heuristic argument for the fact that SW-SSB at the top boundary requires an infinite depth for $0 < p_z < \frac{1}{2}$. On the other hand, the local channel can induce SW-SSB in 2d in finite depth since an "error" membrane will be suppressed for a large but finite depth (see the example in Sec. VA and Appendix. C for discussions).

IV. HOLOGRAPHIC DUALITY FROM ISOTNS

In this section, we elaborate on the holographic duality using the framework of isometric tensor-network states (isoTNS). This framework provides a generic tool to relate SW-SSB steady state and topological order in one higher dimension, offering the possibility to go beyond the simple example considered in the previous section.

We begin by first recalling the mapping between 2d isoTNS and repeated application of a quantum channel on a 1d system. The relation generalizes to higher dimensions straightforwardly. The isoTNS on a square lattice can be described by the local tensor with two physical legs and four virtual legs $T_{ijmn}^{\sigma\gamma}$, with the graphical notation

$$T_{ijmn}^{\sigma\gamma} = i \frac{\gamma}{j} \frac{m}{n}, \qquad (28)$$

where the physical leg labels σ, γ enumerate the local Hilbert space dimension, and the dimension of the virtual legs is referred to as the bond dimension of the tensor networks. By contracting the virtual legs of the adjacent lo-

cal tensors, we obtain a wavefunction with physical sites on the edges of a square lattice (we adopt this convention from Refs.[95–97]). The local tensors of the isoTNS additionally satisfy the following isometry condition

$$\sum_{\sigma,\gamma,m,n} \left(T_{ijmn}^{\sigma\gamma} \right)^* T_{i'j'mn}^{\sigma\gamma} = \delta_{ii'} \delta_{jj'}, \tag{29}$$

where δ denotes the Kronecker delta function. With the isometry condition, we can view the tensor T as the Kraus operators acting on the virtual legs and mapping the legs i,j to the legs m,n. This defines a quantum channel acting on the two-site density matrix defined on the virtual bond space:

$$\Lambda[\rho] = \sum_{\sigma,\gamma} T^{\sigma\gamma} \rho (T^{\sigma\gamma})^{\dagger}. \tag{30}$$

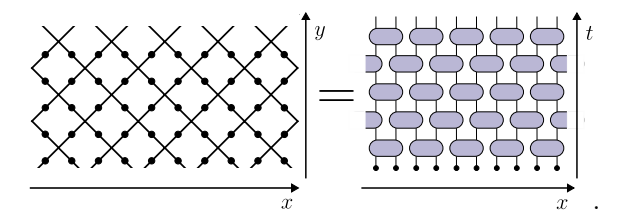
It can be graphically visualized as a double-stacked tensor T acting on the virtual density matrix ρ :

$$\Lambda[\rho] = \sum_{\rho} \equiv \sum_{\rho}, \tag{31}$$

where we simplify the graphical notation at the last step. In particular, the trace-preserving condition of the channel Λ follows from the isometry condition

$$\sum_{\sigma,\gamma} (T^{\sigma\gamma})^{\dagger} T^{\sigma\gamma} = I, \tag{32}$$

where I denotes the identity operator. This shows that the contraction of the bulk of an isoTNS can be understood as a repeated application of the quantum channel Λ on a density matrix defined on the virtual bond space. Conversely, the isoTNS is a particular purification of the repeated quantum channels (Stinspring dilation theorem). Schematically, this channel-state duality in 2d systems can be visualized as



The left-hand side shows the 2d isoTNS, and the right-hand side shows the repeated quantum channel acting on a 1d system, where each purple oval denotes a local quantum channel defined by the isoTNS local tensor T.

It is worth noting that repeated quantum channels are dual to isoTNS, which always represent ground states of frustration-free local Hamiltonians. Physically, the dual isoTNS ground state can be viewed as a superposition of the space—time trajectories generated by the dynamics of the corresponding quantum channel. More precisely,

denote the repeated quantum channel induced by the transfer operator of the isoTNS as $\mathcal{E}[\rho] = \sum_{i} M^{i} \rho(M^{i})^{\dagger}$, where for the isoTNS, i denote the physical degrees of freedom (we group σ, γ in Eq.(30) along each row into i). Suppose the dynamics is initialized with a pure state $|\psi_0\rangle$, then the isoTNS takes the form $\sum_{\{i\},v} c(\{i\},v) |\langle v| \cdots M^{i_3} M^{i_2} M^{i_1} |\psi_0\rangle | |i_1,i_2,i_3,\cdots,v\rangle,$ where v label the virtual degrees of freedom and $c(\{i\},v)$ is some complex phase. Here, we focus only on the unraveling along the temporal direction and ignore the internal structure within each row; those rows encode spatial information, which can be unraveled in an analogous way. In this sense, the isoTNS wavefunction can be viewed as a superposition of all unraveled trajectories of the quantum channel, each weighted by the (square root of) corresponding trajectory probability and an associated complex phase. This duality thus establishes an explicit connection between the properties of the quantum channel and the ground-state ordering in the many-body system.

A. Forced nontrivialness of isoTNS from channel-state duality

A fundamental implication of the channel–state duality is that the strong symmetries of a repeated quantum channel correspond to the virtual symmetries of the isoTNS, which act exclusively on the virtual Hilbert space, spanned by the virtual degrees of freedom of the tensor network. This duality highlights the pivotal role of strong and virtual symmetries in determining, respectively, the emergence of SW-SSB in the channel picture and bulk topological order in the tensor-network picture.

Using the channel–state duality, we provide a physical argument that a generic isoTNS with a nontrivial global virtual symmetry necessarily has a parent Hamiltonian with nontrivial ground-state degeneracy on a cylinder. In two dimensions, when the virtual symmetry is described by a matrix-product-operator (MPO) algebra [98–101], we expect such a generic isoTNS to exhibit topological order. Here, "generic" means that the isoTNS is not fine-tuned and does not possess any additional accidental virtual symmetries. Note that this is in stark contrast to generic tensor-network states (such as projected-entangled pair states (PEPS)), where the presence of MPO virtual symmetries alone is not sufficient to lead to topological order.

Our argument proceeds in two steps. First, we show that the coexistence of the local isometry condition and a nontrivial virtual symmetry guarantees that the transfer operator of the isoTNS has degenerate fixed points. Second, we argue that this fixed-point degeneracy implies ground-state degeneracy of the parent Hamiltonian.

We make use of the channel–state duality by first considering the effect of strong symmetries in quantum channels. The existence of a strong symmetry in a quantum channel necessarily implies a degenerate steady-

state manifold: each symmetry sector of the strong symmetry must contain at least one steady state ¹. Through the channel-state duality, this degeneracy maps to the isoTNS transfer operator, whose fixed-point degeneracy arises from a nontrivial virtual symmetry. To see the physical consequence of this degeneracy, notice that the virtual symmetry acts solely on the virtual legs while leaving the physical degrees of freedom unaffected. Hence, these degenerate fixed points correspond to bulk states with identical energy with respect to the frustration-free local parent Hamiltonian constructed directly from the tensor-network representation (e.g., as described in [98]). Since distinct fixed points indicate that the associated isoTNS wavefunctions are distinct, the parent Hamiltonian of the isoTNS, when defined on a cylinder, possesses degenerate ground states. The argument extends to isoTNS in higher spatial dimensions as well.

The forced nontrivialness directly leads to intriguing physical consequences. For example, if a nontrivial virtual symmetry is preserved, the parent Hamiltonian of the isoTNS cannot possess a unique trivial ground state. Similarly, in the dual channel picture, a strongly symmetric quantum channel cannot have a unique paramagnetic steady state [53, 71]. Importantly, both the isometry condition and the presence of a nontrivial virtual symmetry must coexist; violating either one immediately evades this constraint.

While the discussion above emphasizes physical intuition, the underlying argument can be made mathematically precise in many cases. For 2d tensor-network states, the framework developed in Refs. [98–101] establishes a deep connection between virtual symmetries and topological order. In this setting, one considers a translationally invariant local tensor T defining the tensor networks, and that there exists a virtual symmetry described by an MPO algebra \mathcal{M} on the virtual indices of T. These MPO algebras are precisely the mathematical structures underlying the classification of non-chiral topologically ordered fixed-point states within the tensor-network formalism. The same MPO algebras also classify fixed-point matrix-product density operators (MPDOs) [102–104], which appear as the boundary mixed states associated with 2d non-chiral topological fixed points.

In our setting, the tensor-network states are further constrained to be isoTNS. We thus expect that the resulting isoTNS with these MPO virtual symmetries exhibit

topological order characterized by these MPO algebras. Furthermore, the isoTNS admits a dual interpretation in terms of repeated quantum channels whose strong symmetries are implemented by the same MPO algebra \mathcal{M} . From this perspective, the boundary mixed state produced by the isoTNS can be naturally interpreted as the steady-state manifold of a strongly symmetric channel, realizing the steady-state structure we identify as SW-SSB with respect to the MPO symmetry. The channel-state duality therefore offers a powerful tool to translate the tensor-network theoretic results to classify distinct quantum channels and their steady-state structures.

B. Continuously-tuned quantum channels and U(1) SW-SSB critical point

The isoTNS framework provides a useful tool to extend the holographic correspondence beyond the fixed-point states with zero correlation length, enabling the exploration of continuous deformations and phase transitions between distinct quantum phases and steady states. In particular, recent works have demonstrated that isoTNS with finite bond dimension can represent families of continuously varying ground states across a topological quantum phase transition [95–97]. Through the channel–state duality of isoTNS, such a topological quantum phase transition directly maps onto a continuously tuned transition in the corresponding repeated quantum channels and their steady-state manifolds.

To explicitly construct such a transition path, we employ the plumbing method [95]. In this approach, the local tensor T is required to have the following form

$$T_{ijmn}^{\sigma\gamma} = \sum_{i'j'} \delta_{ii'}^{\gamma} \delta_{jj'}^{\sigma} W_{i'j'mn}, \tag{33}$$

or pictorially,

where $\delta = \Phi$ denotes the Kronecker delta such that it takes the value one when all indices agree, and zero otherwise. With this form, the tensor-network state is entirely specified by the W-tensor. The isometry condition (Eq.29) becomes a normalization condition on the W-tensor as $\sum_{mn} |W_{ijmn}|^2 = 1$ for all i, j. Due to the plumbing δ , the virtual system coincides with the physical system. We introduce a parametrized W-tensor defined for $g \in [-1, 1]$

$$W(g) \propto \begin{bmatrix} 1 & f(g) & f(g) & |g| \\ f(g) & \sqrt{\frac{1+g^2}{2}} & \sqrt{\frac{1+g^2}{2}} & f(g) \\ f(g) & \sqrt{\frac{1+g^2}{2}} & \sqrt{\frac{1+g^2}{2}} & f(g) \\ |g| & f(g) & f(g) & 1 \end{bmatrix}, \quad (34)$$

This follows directly from trace preservation [28]. Given a quantum channel \mathcal{E} , viewed as a linear map acting on operators in the Hilbert space, trace preservation ensures that the identity operator I is always a left eigenvector of \mathcal{E} with eigenvalue 1 $(\mathcal{E}^{\dagger}[I] = I)$. Let P_{λ} denote the projector onto the eigensubspace of the strong symmetry U with distinct eigenvalue λ , satisfying $\sum_{s} P_{s} = I$. Since each P_{λ} commutes with \mathcal{E}^{\dagger} , the operators $P_{\lambda} \cdot I$ form linearly independent left eigenvectors associated with the same eigenvalue 1. Consequently, there must exist the same number of right eigenvectors, i.e., steady states, with eigenvalue

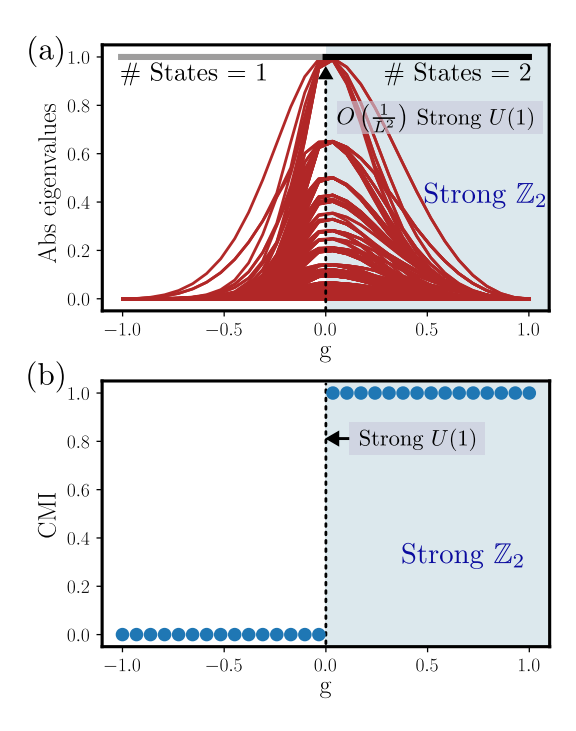


FIG. 6. Tuning a transition in the quantum channel defined from the W tensor in Eq.34. This is equivalent to the transition in the isoTNS under the channel-state duality. The isoTNS is in the toric-code topologically-ordered phase for q > 0 and in the trivial paramagnetic phase for q < 0. The figures present the numerical results based on the exact diagonalization of the transfer matrix that defines the quantum channel for L = 10 with a periodic boundary condition. A strong symmetry \mathbb{Z}_2 is preserved for g > 0. (a) The absolute value of the eigenvalues of the transfer matrix spectrum. The red lines represent the eigenvalues with magnitude less than 1. The steady-state degeneracy is 2 and 1 for q > 0 and q < 0, respectively. At q=0, the channel preserves the strong U(1)symmetry, leading to L+1 steady state degeneracy; the gap closes as $O(1/L^2)$, by mapping the transfer operator to that of the classical six-vertex model [105]. (b) The CMI, in units of log 2, of the steady states computed according to the partition in Fig.4(a), with |A| = |C| = 3 and |B| = 4 (two sites per subregion of B). For g > 0, the steady states are degenerate; we compute the CMI of one of the strongly symmetric steady states.

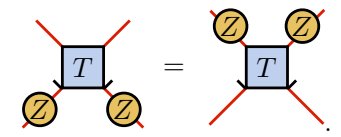
where the indices i, j and m, n are grouped into the row and column of a matrix, respectively. The function f(g) = 0 for $g \ge 0$ and f(g) = |g| for g < 0. By the channel-state duality, this family of isoTNS is dual to a family of continuously-tuned repeated quantum channels.

At g = 1, the isoTNS represents the toric-code ground state, as can be seen from the W-tensor:

$$W_{ijmn} = \begin{cases} 1, \text{ for } i+j+m+n=0 \mod 2\\ 0, \text{ for } i+j+m+n=1 \mod 2 \end{cases}$$
 (35)

with i, j, m, n = 0, 1 denoting the configuration in Pauli-Z basis. As g is tuned away from this limit, the bulk wavefunction has a finite correlation length and exhibits

the same topological order until g=0, where the gap of the transfer operator closes. Importantly, for $g\in[0,1]$, W_{ijmn} remains vanishing for i+j+m+n=1 mod 2, which translates to a virtual \mathbb{Z}_2 symmetry in the isoTNS:



Namely, it is a symmetry acting solely on the virtual (red) legs. Such a local virtual symmetry on a tensor also implies that the isoTNS defines a strongly symmetric quantum channel; given any 1d input pure state with the global symmetry $\prod_i Z_i$, the output state of the channel will have the strong symmetry $\prod_i Z_i$ as well ².

For g < 0, such a virtual symmetry no longer exists. The isoTNS describes a trivial paramagnetic phase and become the product state $|++\cdots\rangle$ at $g=-1^3$. A transition thus happens at q=0, where the transfer matrix defining the quantum channel is exactly that of the critical six-vertex model [105], and the gap closes as $O(1/L^2)$. In particular, there is a U(1) virtual symmetry, corresponding to the particle-number conservation. More concretely, a virtual bond can take the value 0 or 1, which can be interpreted as the absence or presence of a particle. Using the explicit form of the W tensor at g = 0, one can see that the total particle number in the lower two virtual legs is equal to that in the upper two legs. Correspondingly, the bulk isoTNS wavefunction can support an anisotropic power-law correlation along the vertical y direction due to the diffusive dynamics of these U(1) charges, while developing a long-range order along the horizontal direction, with details depending on the choice of the boundary condition [95]. Relatedly, the virtual U(1) symmetry also implies the L+1 exact degeneracy of the transfer matrix, due to the L+1 possible total U(1) charges on a 1d line, which we numerically verify.

Under the channel-state duality, the tunable isoTNS corresponds to a continuously tuned quantum channel with a transition, as shown in Fig.6. At g=1, the isoTNS is the fixed-point toric code, whose top boundary is a steady state (of the corresponding channel) that exhibits \mathbb{Z}_2 SW-SSB. The SW-SSB persists in the range $g \in (0,1]$, which is evident in Fig.6, e.g. indicated by

² Note that although the \mathbb{Z}_2 symmetry here is expressed in a different basis from the one used in Sec. III, generated by $\prod_i X_i$, the two are related by a virtual Hadamard rotation H satisfying HXH=Z and $H^2=I$. This basis change cancels out when the virtual legs are contracted and therefore does not alter the bulk isoTNS wavefunction. In other words, the basis change is merely a "gauge" transformation of the 2d tensor-network state.

³ At g = -1, $W_{ijmn} = 1$ for any i, j, m, n, so the corresponding 2d tensor-network state is a superposition of all Z-basis product state, or equivalently, $|++\cdots\rangle$.

the non-vanishing CMI (conditional mutual information). For g < 0, the isoTNS and the corresponding steady state on the top boundary are in a paramagnetic phase, with CMI = 0. This confirms the validity of the holographic picture beyond the fixed-point limit of the topological wavefunctions. Notably, at g = 0, the virtual Z_2 symmetry is further enhanced to U(1) symmetry, and the channel describes the diffusion of U(1) charges. Correspondingly, given an input pure state with a fixed total U(1) charges, the steady state is a classical mixture of all possible U(1) charge configurations with a fixed total charge, hence exhibiting a U(1) SW-SSB.

Importantly, this transition does not contradict the fact that strongly symmetric quantum channels necessarily possess degenerate steady states, as discussed in the previous section. Consequently, when the symmetry is preserved, one cannot tune a thermodynamic phase transition between a quantum channel with degenerate steady states, including the SW-SSB state, and a quantum channel with a unique steady state. A similar observation was made in Ref. [71], which emphasized that the completely positive and trace-preserving (CPTP) condition forbids a transition from SW-SSB to a paramagnetic phase across different steady states—whether under repeated quantum channels or long-time Lindbladian evolution. Such a transition could only occur by introducing post-selection into the non-unitary process, which necessarily violates the CPTP condition. The present example circumvents this restriction by preserving a strong \mathbb{Z}_2 symmetry of the quantum channel for g > 0, while removing the symmetry for q < 0.

Moreover, the isoTNS framework can be employed to interpolate between the toric code and double-semion ground states, and more generally, between a wide class of string-net states [97]. The presence of distinct bulk topological orders implies that the corresponding dual quantum channels possess distinct SW-SSB steady states. For example, the virtual boundary of the double-semion isoTNS (see Appendix G of [95], and also [97]) will lead to a 1d steady state of the form

$$\rho \propto I + CZX,\tag{36}$$

where the CZX symmetry is defined as CZX = $(\prod_i X_i) (\prod_i CZ_{i,i+1})$ with CZ being the control-Z operator such that $CZ|11\rangle = -|11\rangle$ and it acts trivially otherwise. The intriguing feature is that the anomaly in CZX symmetry implies the steady state ρ is longrange tri-partite entangled: it cannot be created from any tripartite-separable state $\rho_A \otimes \rho_B \otimes \rho_C$ using finitedepth local channels [21]. This is in stark contrast to the SW-SSB steady state ($\propto 1 + \prod_i X_i$) arising from the fixed-point toric-code, which is fully separable (i.e., not entangled). As a notable application, the isoTNS framework provides a concrete protocol to prepare exotic many-body mixed states. For example, one can input any pure state with CZX symmetry (e.g., a GHZ state); applying a depth-1 channel defined by the isoTNS tensor of the double semion will immediately prepare the I+CZX

mixed state. This gives a concrete state-preparation protocol, which would otherwise be difficult to design without the insight of isoTNS. More generally, the continuous tuning of the isoTNS provides an analytically tractable framework for exploring quantum channels with distinct SW-SSB steady states and transitions between them.

V. GENERAL DISCUSSION FOR SW-SSB UNDER HOLOGRAPHIC DUALITY

In this section, we present a variety of examples of SW-SSB, including higher-dimensional generalizations and cases involving various generalized symmetries—such as subsystem and higher-form symmetries—and discuss the corresponding emergent topological orders through holographic duality. The results are summarized in Table II.

A. 2d 0-form SW-SSB

Consider a 2d lattice with one qubit per site, any initial state with the global strong \mathbb{Z}_2 symmetry $\prod_i X_i$ will converge to the SW-SSB state $\propto 1 + \prod_i X_i$ under the repeated application of the noise channel $\mathcal{E} = \prod_{\langle ij \rangle} \mathcal{E}_{ij}^z \prod_i \mathcal{E}_i^x$:

$$\mathcal{E}_{ij}^{z}[\rho_{0}] = (1 - p_{z})\rho_{0} + p_{z}Z_{i}Z_{j}\rho_{0}Z_{i}Z_{j},$$

$$\mathcal{E}_{i}^{x}[\rho_{0}] = (1 - p_{x})\rho_{0} + p_{x}X_{i}\rho_{0}X_{i}.$$
(37)

 \mathcal{E}_{ij}^{x} is a local channel acting on two neighboring qubits and \mathcal{E}_{i}^{x} is a single-site channel. Similar to the discussion in Sec.III, the repeated application of these channels can be understood as a sequential unitary circuit, where the 2d system qubits sequentially interact with the ancilla qubits in the 3d bulk, layer by layer. Tracing out all ancilla qubits then effectively implement the channel acting on the system qubits.

Notably, at $p_x = p_z = \frac{1}{2}$, the 3d bulk has the stabilizers:

$$A_{v} = \begin{array}{c} X \\ X \\ X \end{array} \begin{array}{c} X \\ X \end{array} , \qquad B_{p} = \begin{array}{c} Z \\ Z \\ Z \end{array}$$

$$(38)$$

The vertex stabilizer A_v is a product of 6 Pauli-Zs around a vertex, and the plaquette stabilizer B_p is a product of 4 Pauli-Xs around a plaquette. These stabilizers indicate the 3d toric code, which exhibits a \mathbb{Z}_2 topological order. In addition, the top boundary is specified by the stabilizers

$$A_{v}^{\text{top}} = X X X X , \quad B_{p}^{\text{top}} = Z Z$$

$$(39)$$

Steady state in d-dim	Topological order in $d+1$ -dim
Z_2 0-form SW-SSB in 1d	2d toric code with e-charge-condensed boundary
Z_2 0-form SW-SSB in 2d	3d toric code with e-charge-condensed boundary
Z_2 1-form SW-SSB in 2d	3d toric code with m-loop—condensed boundary
Z_2 subsystem SW-SSB in 2d	3d fracton order with charge-condensed boundary
Z_2 fermionic 0-form SW-SSB in 1d	2d toric code with boundary condensation of f -charges and Majorana fermions.
\mathbb{Z}_2 fermionic 1-form SW-SSB in 2d	3d fermionic toric code with flux-loop-condensed surface

TABLE II. Various examples that illustrate the holographic duality between SW-SSB and topological orders.

where the system qubits (i.e., the output state of the repeated quantum channel) are colored in red.

Away from this maximal decoherence limit, i.e. $p_x, p_z \neq \frac{1}{2}$, one instead obtains a deformed toric code

$$|\text{TC}\rangle (g_x, g_z) = \prod_{\ell \in x - y \text{ plane}} e^{g_z X_\ell} \prod_{\ell \in z \text{ link}} e^{g_x Z_\ell} |\text{TC}\rangle, (40)$$

with

$$e^{2g_z} = \frac{1 - p_z}{p_z} \; , \quad e^{2g_x} = \frac{1 - p_x}{p_x} .$$
 (41)

Here the imaginary evolution $e^{g_x X_\ell}$ occurs on all links on the x-y plane, and $e^{g_x Z_\ell}$ occurs on the z-link. The \mathbb{Z}_2 topological order will be robust under these deformations, unless $g_z \to \infty$ or $g_x \to \infty$, which corresponds to the zero-noise limit $p_z = 0$ or $p_x = 0$. This wavefunction is defined on a 3d lattice with periodic boundary conditions along x,y directions, and with open boundaries along z. The reduced density matrix on the top surface (say $z = L_z$) is the output steady state of the repeated applications of the channel.

At the fixed point limit $(p_x = p_z = \frac{1}{2})$, a string operator of Pauli-Zs generates the two e-charges on the two endpoints of the string. Notably, the Z-type boundary stabilizer in Eq.39 indicates that the top surface realizes an e-condensed boundary, where a pair of e-charges can condense on the boundary. Such e-condensation also gives rise to the weak symmetry for the SW-SSB state ρ on the boundary: $Z_i Z_j \rho Z_i Z_j = \rho$, where i, j can be any two points on the top surface.

On the other hand, one can define a non-contractible closed-membrane operator on the top surface:

$$V_{\text{surface}} = \prod_{i \in \text{surface}} X_i,$$

which measures the global m-flux and generates the associated \mathbb{Z}_2 1-form symmetry. Since the wavefunction in Eq.40 is an eigenstate of V_{surface} for all finite g_x, g_z , the reduced density matrix on the top surface has a strong \mathbb{Z}_2 symmetry. Thus, under the holographic duality, the strong symmetry of the 2d boundary reduced state descends from the 1-form symmetry in the 3d bulk.

Unlike the 1d case discussed in Sec.III, which requires an infinite depth to realize SW-SSB with non-maximal decoherence, the channel acting on the 2d lattice can drive a transition to the SW-SSB phase with a finite constant depth, even with non-maximal decoherence [55, 56]. Heuristically, this is because the Z string operator with two endpoints on the top boundary can emerge at finite depth. We provide a more detailed discussion about this perspective in Appendix.C.

B. 2d 1-form SW-SSB

Consider a 2d lattice with qubits defined on edges, one can define the \mathbb{Z}_2 1-form symmetry generator $B_p = \prod_{\ell \in \partial p} X_\ell$, which is the product of four Xs along a plaquette p. These B_p operators generate the 1-form symmetry: $\prod_{\ell \in \mathcal{C}} X_\ell$, which is the product of Xs along any closed (contractible) loop \mathcal{C} . A canonical example of the mixed state, where the strong 1-form symmetry is spontaneously broken down to the weak one, is the maximally mixed state with this strong 1-form symmetry [60, 69]:

$$\rho \propto \prod_{p} (1 + B_p). \tag{42}$$

An essential feature of this mixed state is the existence of the weak 1-form symmetry along loops in the dual lattice, which is generated by

$$A_v = \prod_{\ell \in v} Z_\ell,\tag{43}$$

namely, the product of four Zs around a vertex v. The universal feature of the SW-SSB can then be understood as the mutual anomaly between the strong X loops and the weak Z loops.

Again, to develop a holographic description, we will consider a repeated quantum channel that (i) preserves a strong higher-form symmetry and (ii) allows for a weak higher-form symmetry to emerge in the steady state. Concretely, we define the following quantum channel $\mathcal{E} = \prod_{v} \mathcal{E}_{v}^{z} \prod_{\ell} \mathcal{E}_{\ell}^{\ell}$, with

$$\mathcal{E}_{\ell}^{x}[\rho] = (1 - p_x)\rho + p_x X_{\ell}\rho X_{\ell}.$$

$$\mathcal{E}_{v}^{z}[\rho] = (1 - p_z)\rho + p_z A_v \rho A_v$$
(44)

 \mathcal{E}_{ℓ}^{x} is an X-dephasing channel, and \mathcal{E}_{v}^{z} is the channel that applies the star operator A_{v} defined in Eq.43 with probability p_{z} . It is straightforward to check that the decoherence channel \mathcal{E} preserves the strong X 1-form symmetry. In particular, starting from any pure state with the X 1-form symmetry, it will converge to the SW-SSB mixed state defined in Eq.42.

Building on our holographic framework, where the repeated quantum channel is viewed as a sequential unitary circuit that generates a wavefunction in one higher dimension, we find that the bulk ancilla qubits form a 3d \mathbb{Z}_2 topological order (see Appendix.E for details). In particular, at $p_x = p_z = \frac{1}{2}$ corresponds to the fixed-point limit, described by the toric-code stabilizer in the bulk

$$A_v = \begin{array}{c} Z \\ Z \\ Z \\ Z \end{array}, \quad B_p = \begin{array}{c} X \\ X \\ X \end{array}$$

$$(45)$$

Notably, the steady state (Eq.42) of the repeated quantum channel in Eq.44 is the reduced density matrix on the top boundary of the 3d toric code with a smooth (m-loop-condensed) surface, as shown in Fig.7. In this holographic picture, the strong symmetry of the steady state descends from a bulk 2-form symmetry (i.e., the product of Pauli-Xs along any 1d closed loops). On the other hand, the weak symmetry originates from a bulk 1-form symmetry whose membrane operators pierce the bulk and intersect the surface as loops. Consequently, the mixed anomaly between the strong and weak 1-form symmetries in the steady state is inherited from the topological order of the 3d bulk.

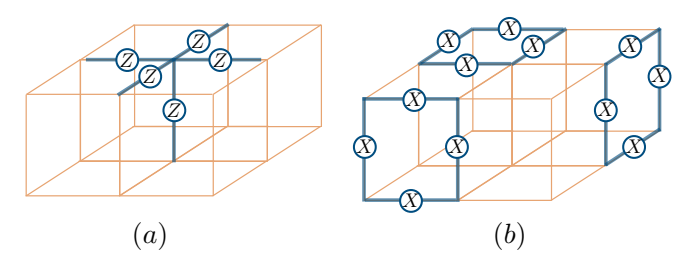


FIG. 7. The surface stabilizers for the 3d toric code emerging from the repeated quantum channel (Eq.44). (a) The Z-type stabilizer indicates the condensation of the magnetic-flux (m) excitation on the top surface. Tracing out the bulk leads to the weak-1-form symmetry of the top-surface reduced density matrix. (b) The top surface has the $X^{\otimes 4}$ stabilizer, leading to the strong 1-form symmetry of the top-surface reduced density matrix.

C. 2d subsystem SW-SSB

We here discuss a novel SW-SSB state in 2d with strong subsystem symmetries, and show that it is holographically dual to a topological fracton model in 3d. To begin, we consider a 2d lattice with one qubit per site, and define the following subsystem symmetries:

$$U_x = \prod_{y=1}^{L_y} X_{x,y}, \quad U_y = \prod_{x=1}^{L_x} X_{x,y}.$$
 (46)

 U_x and U_y act on the 1d lines along the vertical (y) direction and the horizontal (x) direction, respectively.

The maximally mixed state with these subsystem symmetries is

$$\rho_{\text{sub}} \propto \prod_{x} (1 + U_x) \prod_{y} (1 + U_y) \tag{47}$$

In particular, ρ_{sub} is weakly symmetric under W_{x_1,x_2,y_1,y_2} defined as

$$W_{x_1, x_2, y_1, y_2} = Z_{x_1, y_1} Z_{x_2, y_1} Z_{x_2, y_2} Z_{x_1, y_2}, \qquad (48)$$

which is the product of four Pauli-Zs on the corners of a rectangle. The SW-SSB can be understood as the mutual anomaly between the strong subsystem symmetries U_x, U_y and the weak symmetry W_{x_1, x_2, y_1, y_2} . This mixed state can be obtained by the repeated ac-

This mixed state can be obtained by the repeated action of the channel $\mathcal{E} = \prod_{P} \mathcal{E}_{P}^{z} \prod_{i} \mathcal{E}_{i}^{x}$, with

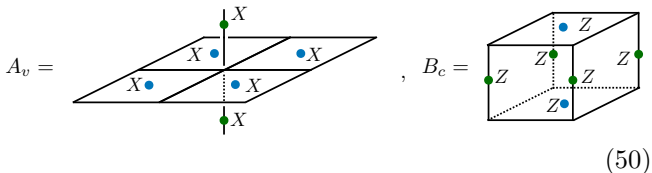
$$\mathcal{E}_{P}^{z}[\rho_{0}] = (1 - p_{z})\rho_{0} + p_{z}(\prod_{i \in P} Z_{i})\rho_{0}(\prod_{i \in P} Z_{i}).$$

$$\mathcal{E}_{i}^{x}[\rho_{0}] = (1 - p_{x})\rho_{0} + p_{x}X_{i}\rho_{0}X_{i},$$
(49)

where $\prod_{i \in P} Z_i$ denotes the product of four Pauli-Zs on the corners of a plaquette P.

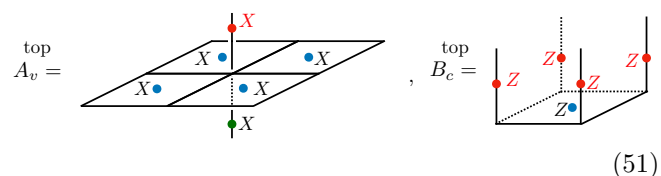
This channel can be realized as a sequential circuit where the 2d system qubits sequentially interact with the ancilla qubits on the plaquette on the x-y plane (responsible for \mathcal{E}_P^z channel) and the ancilla qubits on the z-direction link (responsible for \mathcal{E}_i^x channel).

At $p_z = p_x = \frac{1}{2}$, the 3d bulk theory is described by two types of 6-body stabilizers:



 A_v is the product of the two Xs on the z-directional link and the four Xs on the x-y plane plaquettes neighboring the vertex v. B_c is the product of the four Zs on the z-directional links and the two Zs on the x-y plane plaquettes in the cube c. This is an anisotropic fracton model with lineons and planons, first discovered in Ref.[106]. It represents a foliated fracton phase with 2 foliations composed of toric code layers along the x-z and y-z planes.

The top boundary is specified by the following stabilizers:



where the red qubits are the output of the repeated quantum channel. Those red qubits have the strong subsystem symmetries U_x , U_y in Eq.46, and the weak symmetry comes from tracing out the bulk qubits given the $B_c^{\rm top}$ stabilizer. In particular, the boundary condition specified by $B_c^{\rm top}$ indicates that four electric lineons condense on the top boundary (see Ref.[106, 107] for details on the lineon excitations).

D. 1d fermion parity SW-SSB

Here, we apply our holographic framework to study SW-SSB in a fermionic system. Consider a one-dimensional fermionic chain with two Majorana modes per site, η_i and η'_i . The system possesses a global \mathbb{Z}_2^f symmetry generated by $\prod_i P_i$, where $P_i = -i\eta_i\eta'_i$ denotes the onsite fermion parity. We focus on an SW-SSB state ρ_f , in which the strong \mathbb{Z}_2^f symmetry is spontaneously broken down to the weak \mathbb{Z}_2^f :

$$\rho_f \propto 1 + \prod_i P_i. \tag{52}$$

The essential properties of ρ_f are (i) the strong Z_2^f symmetry $\prod_i P_i$ and (ii) the weak 1-form symmetry $\eta_i' \eta_j \rho_f \eta_j \eta_i' = \rho_f$. The SW-SSB follows from the mutual anomaly between the strong and weak symmetries. Below, we will show that it is holographically dual to a toric-code order in 2d, with a key feature that the condensed boson on the 1d boundary is a composite of a physical Majorana and a fermionic excitation of the toric code.

To obtain a holographic description, we consider the repeated action of the channel:

$$\mathcal{E}_{i}^{a}[\rho_{0}] = (1 - p_{z})\rho_{0} + p_{z}\eta_{i}'\eta_{i+1}\rho_{0}\eta_{i+1}\eta_{i}'$$

$$\mathcal{E}_{i}^{b}[\rho_{0}] = (1 - p_{x})\rho_{0} + p_{x}P_{i}\rho_{0}P_{i}.$$
(53)

This quantum channel can be viewed as the Jordan–Wigner transformation of the Ising quantum channel in Eq.6. Given this duality, the channel admits a sequential-circuit realization: ancilla qubits on the x and y links form a toric-code wavefunction in the bulk, while the Majorana degrees of freedom on the boundary vertices couple to the ancilla qubits in the bulk. (see Fig.8).

At $p_x = p_z = \frac{1}{2}$, the bulk qubits form the fixed-point toric code state, and the boundary coupling between the Majorana fermions and qubits is indicated by the $\eta' X \eta$

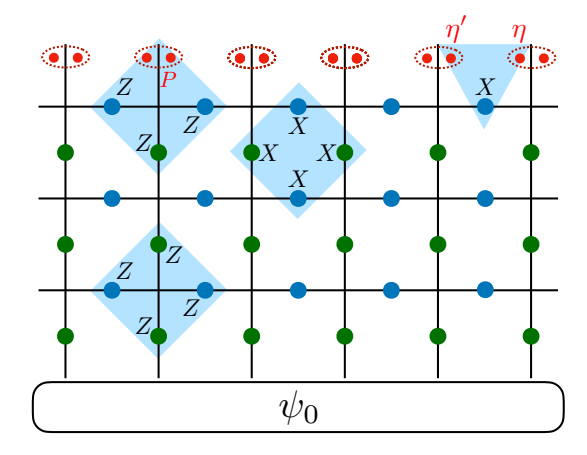
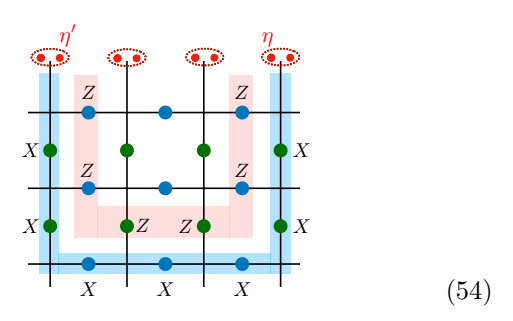


FIG. 8. Holographic duality between the \mathbb{Z}_2^f SW-SSB on the top boundary and the bulk \mathbb{Z}_2 topological order. At $p_x = p_z = \frac{1}{2}$, the bulk is the fixed-point toric code with the star stabilizer $A_v = Z^{\otimes 4}$ and plaquette stabilizer $B_p = X^{\otimes 4}$.

type stabilizer (the phase is omitted) and PZZZ type stabilizer. Notably, the combination of these two types of stabilizers implies the long-string stabilizer, where the two boundary Majoranas are connected by a fermion string - a composite object of the X string and Z string - through the bulk, shown as follows:



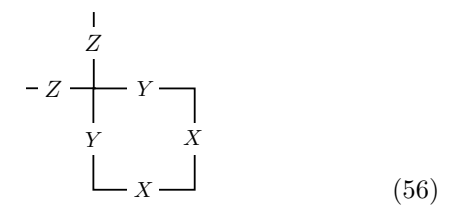
In other words, the fermion charges from the toric code bind with a physical Majorana fermion to form a composite bosonic particle that condenses on the 1d top boundary. When tracing out the bulk to obtain the boundary density matrix ρ_f , such a strong fermion-line symmetry becomes a weak fermionic symmetry: $\eta_i'\eta_j\rho_f\eta_j\eta_i'=\rho_f$, which together with the strong symmetry $\prod_i P_i$ indicates the 1d SW-SSB.

E. 2d fermionic 1-form SW-SSB

As our final example, we consider a quantum channel whose steady state realizes an intrinsically mixed-state topological order [23, 24], namely the fermion-decohered toric code, defined as [41]

$$\rho_f \propto \prod_v (1 + A_v B_{p(v)}). \tag{55}$$

 $A_v = Z^{\otimes 4}$ is the product of four Pauli-Zs around a vertex, and $B_p = X^{\otimes 4}$ is the product of four Pauli-Xs around a plaquette. In particular, $B_{p(v)}$ is the bottom-right plaquette adjacent to the vertex v, so the stabilizer $A_v B_{p(v)}$ takes the form



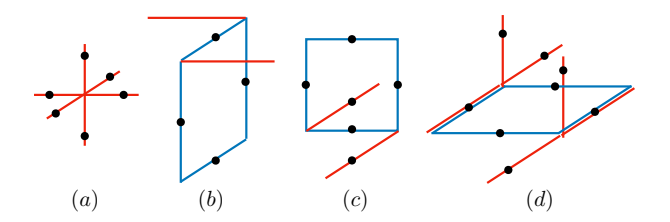
These stabilizers define the standard fermionic 1-form symmetry in the 2d toric code: $\prod_{\ell \in \mathcal{C}} Z_{\ell} X_{\ell + \frac{\hat{x}}{2} - \frac{\hat{y}}{2}}$, with \mathcal{C} being any closed loops. When cut open, it creates the f excitation (the e-m bound state) on the two endpoints of the string.

To generate ρ_f starting from any pure state with fermionic 1-form symmetry, we consider the repeated application of the channel $\mathcal{E} = \prod_v \mathcal{E}_v \prod_\ell \mathcal{E}_\ell$ with

$$\mathcal{E}_{\ell}[\rho] = p_{\ell}\rho + (1 - p_{\ell})X_{\ell}Z_{\ell + \frac{\hat{\pi}}{2} - \frac{\hat{y}}{2}}\rho X_{\ell}Z_{\ell + \frac{\hat{\pi}}{2} - \frac{\hat{y}}{2}}
\mathcal{E}_{v}[\rho] = p_{v}\rho + (1 - p_{v})A_{v}\rho A_{v}$$
(57)

When $p_{\ell}, p_{v} \neq 0$, ρ_{f} is the unique steady state in the strong fermionic 1-form symmetry section.

Notably, at $p_{\ell} = p_v = \frac{1}{2}$, the corresponding 3d holographic wavefunction is described by the following stabilizers, akin to the 3d fermionic toric code discussed in Ref. [108–112]:



The qubits defined on the x-y plane are the ancilla qubits responsible for \mathcal{E}_{ℓ} noise, and the qubits defined on the z-direction (vertical) links are the ancilla qubits responsible for \mathcal{E}_v noise. We use the red line and blue line to label the location of the Pauli-Z and Pauli-X. For example, the stabilizer (a) is a vertex term of the form $Z^{\otimes 6}$. In stabilizer (d), the simultaneous presence of blue and red lines indicates the coexistence of Pauli-X and Pauli-Z, or equivalently, the Pauli-Y. One can check that all the stabilizers commute with each other.

The top boundary, which corresponds to the steady state in 2d, is specified by the stabilizers shown in Fig.9. The truncated vertex-type operator implies the m-flux condensation, and it gives rise to the weak symmetry $A_v \rho_f A_v = \rho_f$ of the 2d boundary reduced density matrix; see Fig.9(a). On the other hand, the stabilizer in Fig.9(b) acts purely on the top surface, corresponding to the strong fermionic 1-form symmetry.

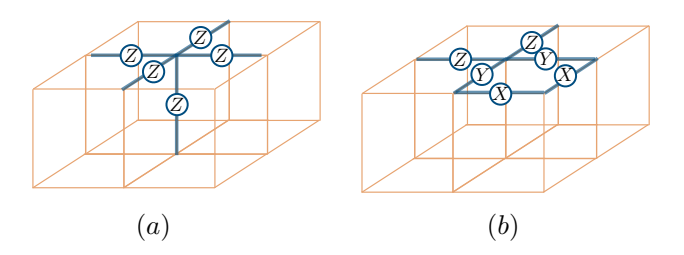


FIG. 9. Surface stabilizers of the fermionic toric code. The stabilizer in (a) indicates the condensation of m-flux-loop excitations, which gives rise to the weak 1-form symmetry upon tracing out the bulk qubits. The stabilizer in (b) is exactly the one in Eq.56, which gives the strong fermionic 1-form symmetry on the 2d surface.

F. SW-SSB from non-CPTP maps

In this manuscript, we primarily focus on the steady states arising in strongly symmetric quantum channels and demonstrate that such mixed states can be holographically dual to the boundary of higher-dimensional topological (fracton) order. Within this holographic framework, the time evolution of a d-dimensional quantum channel is dual to the transfer matrix of an isometric tensor network wavefunction in higher dimensions.

Our holographic perspective can be further extended to scenarios beyond quantum channels and general CPTP (completely positive and trace-preserving) maps in open systems. For instance, consider a non-unitary process where the system interacts with ancilla qubits and the ancilla are subsequently post-selected. Such dynamics are not CPTP [113–115], yet if this process is repeated infinitely many times, the system can still relax to a steady state that exhibits strong-to-weak symmetry breaking (SW-SSB). Remarkably, even in these non-CPTP scenarios, the resulting non-unitary time evolution can still be encoded as the transfer matrix of a higher-dimensional tensor network wavefunction, although the network need not be of the isoTNS form. Hence, our duality framework establishes a unified viewpoint: many mixed states arising in open quantum systems, regardless of whether the underlying evolution is CPTP, can be viewed either as reduced density matrices (RDM) of higher-dimensional wavefunctions, or as the virtual bonds of higher-dimensional tensor network states. The strong symmetry conditions imposed on the quantum channel translate into constraints on the tensor symmetries in the higher-dimensional wavefunction, such as emergent 1-form symmetries. Conversely, starting from a nontrivial (topologically ordered) wavefunction, one can always examine its reduced density matrix as a lower-dimensional mixed state [116]; in such cases, a 't Hooft anomaly associated with the bulk topological order guarantees that the RDM exhibits SW-SSB.

We anticipate that our holographic framework will have broader implications for the structure of mixed-state ensembles and the reduced density matrices of topologically ordered systems in higher dimensions. To illustrate this explicitly, we consider the boundary RDM of the toric code state with homogeneous string tension $|\psi(\beta)\rangle \propto \prod_i e^{\beta Z_i} |\text{TC}\rangle$ [85, 86]. While this deformed state admits a tensor-network representation of finitebond dimension, the tensor work is not an exact isoTNS. Hence, the corresponding transfer matrix does not define a CPTP channel. This is in contrast to the toric code with inhomogeneous deformation in Sec. III A, which admits an isoTNS representation. As β is varied, the deformed state $|\psi(\beta)\rangle$ transitions from \mathbb{Z}_2 topological order to a topologically trivial phase at a critical β . We numerically examine the CMI (conditional mutual information) of the boundary RDM across this topological phase transition. The results are shown in Fig.10. As the system size increases, the boundary CMI exhibits a sharpening jump from the trivial zero to log 2 across the phase transition, consistent with the holographic picture.

VI. OUTLOOK

To summarize, we propose a holographic correspondence between steady states with SW-SSB and topologically ordered states in one higher dimension. Our results show that a mixed state under repeated noise can be viewed as the RDM of a higher-dimensional wavefunction represented by an isoTNS. Theoretically, this holographic duality allows us to infer salient features of SW-SSB mixed states, including long-range CMI and non-local recoverability, from the corresponding topological order. Conversely, since any quantum channel admits an isoTNS dual, the duality provides a route to classify and analyze steady-state transitions by manipulating the virtual bonds of the isoTNS.

In this work, we have mostly focused on SW-SSB of discrete symmetries; extending the framework to various continuous symmetries [53, 117, 118] remains open. In particular, Refs. [50, 119] reports that a strongly SU(2) symmetric 1d quantum channel can exhibit steady states whose bipartite mixed-state entanglement (e.g. entanglement of formation [120] and logarithmic negativity [121– 124) scales logarithmically with size. It would be illuminating to identify the associated bulk wavefunction and infer steady-state entanglement from the holographic dual. Likewise, quantum channels with strong continuous symmetry can host hydrodynamic modes [53, 117] with gapless transfer-matrix spectra and long mixing times; clarifying how these features manifest in the holographic bulk is an essential next step. Meanwhile, recent developments have shown that there is no chiral steady state in CPTP evolution, a result that can be proved via channel-circuit duality [125]. It would be illuminating to see how these constraints shed light on isoTNS states.

As discussed in Sec.IV, the framework of isoTNS provides a powerful tool to explore steady-state mixed-state phases and their transitions. For instance, Refs.[95, 97] constructed an isoTNS path that interpolates between

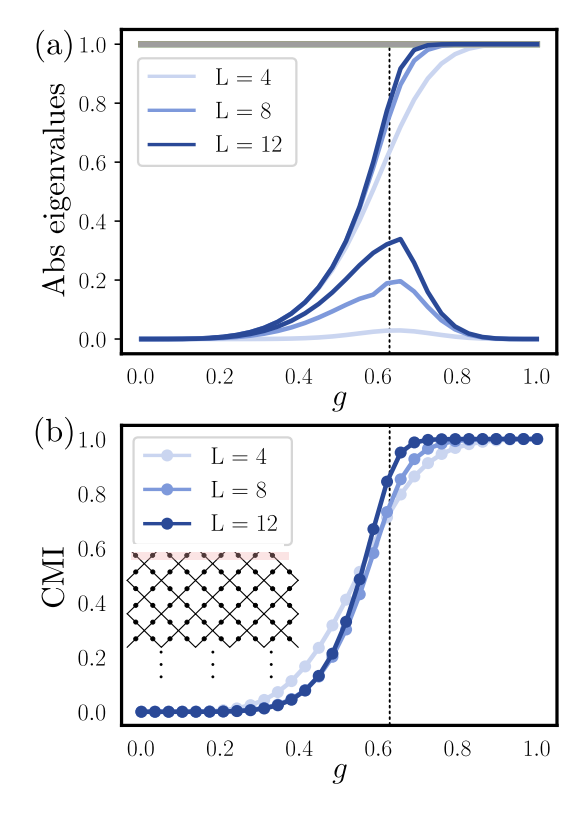


FIG. 10. Topological phase transition and boundary CMI of the deformed toric code with string tension $\prod_i e^{\beta Z_i} |\text{TC}\rangle$ on an $L \times \infty$ cylinder, where $\beta(g) = -\log g$. A transition from \mathbb{Z}_2 topological order to the trivial phase happens at $g_c \approx 0.63$ (dashed line), solved by a mapping to the classical 2D Ising model. The results are obtained from the exact diagonalization of the transfer operator (constructed with the same orientation convention as in Sec. IV, see also the inset panel) of the deformed toric code for different circumference L. The transfer operator is a channel with a strong \mathbb{Z}_2 symmetry; it is, however, not trace-preserving and therefore not a quantum channel. (a) The absolute value of the three eigenvalues closest to 1 (including the eigenvalue 1 itself, marked as a gray line). The gap tends to zero with increasing system size at the critical point. (b) The CMI (in units of log 2) of the boundary subsystem computed according to the partition in Fig.4.

the \mathbb{Z}_2 toric-code topological order and the \mathbb{Z}_2 double-semion topological order, with a continuous transition between them. Viewing the isoTNS as a repeated quantum channel immediately leads to the identification of two distinct 1d mixed-state phases separated by a mixed-state transition—an insight that would otherwise be difficult to obtain. One immediate open question is to develop a complete theory for this intriguing mixed-state quantum criticality. More broadly, the isoTNS framework may provide a unifying platform for uncovering and classifying a wide range of mixed-state phenomena.

Note added.— During the preparation of the manuscript, we became aware of several independent works addressing related topics [116, 125, 126].

ACKNOWLEDGMENTS

We thank Michael Knap for helpful discussions. This research was completed in part by grant NSF PHY-2309135 to the Kavli Institute for Theoretical Physics (KITP). TCL acknowledges the support of the RQS post-doctoral fellowship through the National Science Foundation (QLCI grant OMA-2120757). YJL acknowledges support from the MIT Center for Theoretical Physics - a Leinweber Institute, NSF CIQC Award No. 10434 and NSF Early Career DMR-2237244. YY acknowledges support from NSF under award number DMR-2439118.

Appendix A: Derivation of the deformed toric code

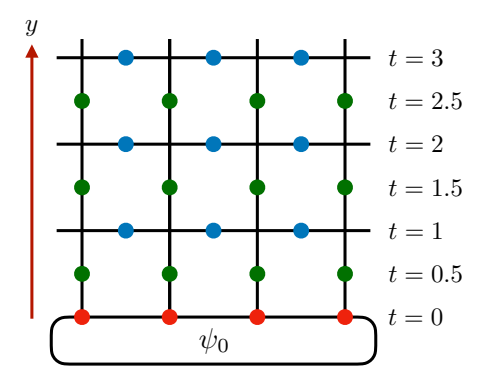
Given the quantum channel $\mathcal{E} = \prod_i \mathcal{E}_i^z \mathcal{E}_i^x$ acting on a 1d system, with

$$\mathcal{E}_{i}^{z}[\rho_{0}] = (1 - p_{z})\rho_{0} + p_{z}Z_{i}Z_{i+1}\rho_{0}Z_{i}Z_{i+1}.
\mathcal{E}_{i}^{x}[\rho_{0}] = (1 - p_{x})\rho_{0} + p_{x}X_{i}\rho_{0}X_{i},$$
(A1)

we show that the repeated application of this channel gives rise to a deformed toric-code wave function in two spatial dimensions.

For simplicity, we first consider the channel at $p_x = p_z = \frac{1}{2}$ to illustrate the emergence of a fixed-point toric code state. The derivation for the general p_x and p_z will be discussed later.

As we have discussed in the main text, a repeated quantum channel acting on the 1d system is a process where this 1d system propagates upward to sequentially interact with ancilla qubits row-by-row, as shown in the following figure:



In other words, system (red) qubits are initialized in the state $|\psi_0\rangle$ at time t=0, and they travel along the vertical y direction to entangle with the green and blue qubits, which are responsible for X noise and ZZ noise, at various time slices. Note that the spatial (y) direction can also be identified as the temporal direction, so we may use y or t interchangeably. For instance, in the figure above, we use t to label the ancilla qubits at various rows; $t=0.5, 1.5, 2.5 \ldots$ label the time slices when the system

(red) qubits interact with the ancilla qubits responsible for the X noise, and $t=1,2,3\ldots$ label the time slices when the system (red) qubits interact with the ancilla qubits responsible for the ZZ noise.

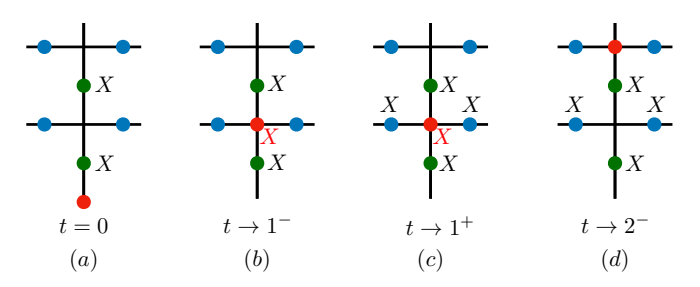


FIG. 11. Evolution of XX stabilizers to the star operator $A_v = X^{\otimes 4}$ under the sequential circuit, at various time slices.

As discussed in the main text, at $p_x = p_z = \frac{1}{2}$, the green and blue qubits are initialized at $|+\rangle$ and $|\bar{0}\rangle$, respectively. To see the emergence of the stabilizer $A_v =$ $X^{\otimes 4}$ under the sequential unitary circuit, we notice that at t=0, since the green qubits are initialized at $|+\rangle$, the initial state has the product of two Pauli-Xs as a stabilizer acting on the two green qubits as shown in Fig.11(a). Next, the red qubit will entangle with the green qubit at t = 0.5 via the controlled gate: $|0\rangle\langle 0|_a + |1\rangle\langle 1|_a X_s$, where a and s refers to the ancilla (green) qubit and system (red) qubit, respectively. Under the conjugation of this gate, the red qubit will be attached by an X operator, so the original XX stabilizer at t=0 becomes an XXX stabilizer, which will remain up to the time $t \to 1^-$, i.e., right before interacting with the blue qubits (Fig. 11(b)). At the time t=1, the red qubit is entangled with the left and right neighboring blue qubits, both using the controlled-gate $|+\rangle \langle +|_a + |-\rangle \langle -|_a Z_s$, implying the stabilizer will be further attached with two Pauli-Xs on those blue qubits (Fig.11(c)). After this, the red qubit will entangle with the green qubit at t = 1.5 using the controlled gate $|0\rangle\langle 0|_a + |1\rangle\langle 1|_a X_s$, which will annihilate the Pauli-X on the system red qubit (Fig.11(d)). Therefore, the original two-body XX stabilizer is mapped to the star operator $A_v = X^{\otimes 4}$ under the sequential circuit.

Now we follow a similar strategy to show the emergence of the plaquette stabilizer $B_p = Z^{\otimes 4}$ under the sequential circuit. At t=0, since all the blue qubits are in the state $|0\rangle$, one can define the ZZ stabilizer on the two blue qubits shown in Fig.12(a). At t=1, the two red qubits are entangled with the blue qubit in between, both using $|+\rangle \langle +|_a + |-\rangle \langle -|_a Z_s$, after which the ZZ stabilizer is decorated by two Z operators on the red qubits (Fig.12(b)). Then, those two red qubits will entangle with the two green qubits at t=1.5. This will generate Pauli-Zs on the green qubits, so one has a sixbody stabilizer (Fig.12(c)). Finally, at t=2, the red qubits interact with the blue qubit in between, leading to the emergence of the four-body plaquette stabilizer $B_p = Z^{\otimes 4}$ (Fig.12(d)).

Therefore, at $p_x = p_z = \frac{1}{2}$, that repeated quantum

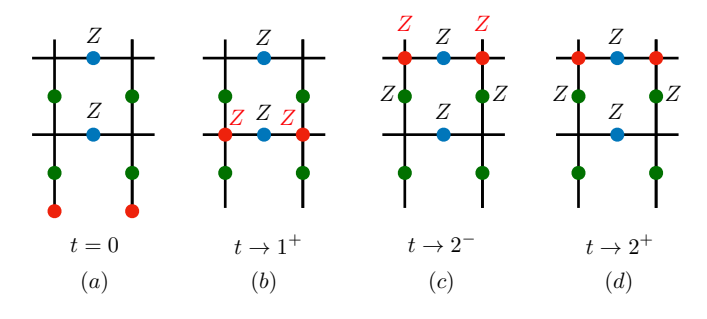


FIG. 12. Evolution of ZZ stabilizers to the plaquette operator $B_p = Z^{\otimes 4}$ under the sequential circuit, at various time slices.

channel is exactly a sequential unitary circuit U that prepares a toric code

$$|\text{TC}\rangle = U \left[|\psi_0\rangle_s \prod_{a \in \text{x-link}} |0\rangle_a \prod_{a \in \text{y-link}} |+\rangle_a \right], \quad (A2)$$

where $|\psi_0\rangle_s$ is the initial state of the system qubits, and the ancilla qubits in horizontal edges (x-links) and vertical edges (y-links) are initialized at $|0\rangle$ and $|+\rangle$, respectively.

Away from $p_x = p_z = \frac{1}{2}$, the corresponding channel can be implemented by deforming the initial state (Eq.10 and Eq.15):

$$|\psi_0\rangle_s \prod_{a\in\text{x-link}} e^{g_z X_a} |+\rangle_a \prod_{a\in\text{y-link}} e^{g_x Z_a} |0\rangle_a$$
 (A3)

where the ancilla qubits are deformed with the imaginary time evolution $e^{g_z X_a}$ or $e^{g_x Z_a}$ with

$$e^{2g_z} = \frac{1 - p_z}{p_z}, \ e^{2g_x} = \frac{1 - p_x}{p_x}.$$
 (A4)

Given the above deformed initial state, the sequential unitary circuit U generates the following pure state $|\Psi^{2d}(g_x, g_z)\rangle$:

$$|\Psi^{2d}(g_x, g_z)\rangle$$

$$= U \left[|\psi_0\rangle_s \prod_{a \in \text{x-link}} e^{g_z X_a} |+\rangle_a \prod_{a \in \text{y-link}} e^{g_x Z_a} |0\rangle_a \right].$$
 (A5)

The reduced density matrix obtained by tracing out all the ancilla qubits is the output of the repeated quantum channel.

Notably, in the sequential circuit U, the x-link ancilla qubits are entangled by the X-basis controlled-gate $|+\rangle \langle +|_a + |-\rangle \langle -|_a Z_s$, so the deformation $e^{g_z X_a}$ commutes with U. Similarly, the y-link ancilla qubits are entangled by the Z-basis controlled gates $(|0\rangle \langle 0|_a + |1\rangle \langle 1|_a X_s)$, so the deformation $e^{g_x Z_a}$ commutes with U

as well. Therefore, those imaginary time evolutions can be pushed to the left of U, implying (using Eq.A2):

$$|\Psi^{2d}(g_x, g_z)\rangle = \prod_{a \in \text{x-link}} e^{g_z X_a} \prod_{a \in \text{y-link}} e^{g_x Z_a} |\text{TC}\rangle, \quad (A6)$$

which is a deformed toric-code state shown in Eq.18.

Appendix B: Absence of finite-g transition

Given the deformed toric code

$$|\Psi^{2d}(g_x, g_z)\rangle = \prod_{\ell \in x \, \text{link}} e^{g_z X_\ell} \prod_{\ell \in y \, \text{link}} e^{g_x Z_\ell} |\text{TC}\rangle, \quad (\text{B1})$$

here we show that its wavefunction overlap is analytic for any finite g_x, g_z , implying the absence of a transition. First, the wavefunction overlap is written as

$$\langle \Psi^{2d}(g_x, g_z) | \Psi^{2d}(g_x, g_z) \rangle$$

$$= \langle \text{TC} | \prod_{\ell \in x \text{ link}} e^{2g_z X_\ell} \prod_{\ell \in y \text{ link}} e^{2g_x Z_\ell} | \text{TC} \rangle$$

$$\propto \langle \text{TC} | \prod_{\ell \in x \text{ link}} (1 + t_z X_\ell) \prod_{\ell \in y \text{ link}} (1 + t_x Z_\ell) | \text{TC} \rangle$$
(B2)

with $t_x \equiv \tanh(2g_x), t_z \equiv \tanh(2g_z)$.

The term $\prod_{\ell \in y \text{ link}} (1 + t_x Z_\ell)$ can be expanded as a sum of all possible Pauli-Z insertions on y-links. Crucially, whenever those Zs do not form a closed loop, they will violate $X^{\otimes 4}$ and create e charges on vertices, and hence, have vanishing contribution in the expectation value w.r.t. $|\text{TC}\rangle$. Only those Zs that extend from the top to the bottom boundaries may have a non-vanishing contribution. The weight of a given extended Z-string decays exponentially with the vertical lattice size L_y (for any finite g_x, g_z), but the multiplicity is only polynomial in the horizontal lattice size L_x . Therefore, the contributions of these extended Z-strings will vanish in the thermodynamic limit (fixed $\frac{L_x}{L_y}$ and $L_y \to \infty$). Similar reasoning holds for $\prod_{\ell \in x \text{ link}} (1 + t_z X_\ell)$. Therefore, the wavefunction overlap will follow

$$\langle \Psi^{2d}(g_x, g_z) | \Psi^{2d}(g_x, g_z) \rangle = 1 + \dots$$
 (B3)

where all terms in ... will vanish in the thermodynamic limit, for finite g_x, g_z .

Appendix C: Emergence of SW-SSB at finite depth

We here present a heuristic argument to show that for the non-maximal decoherence channel $(p_z \neq \frac{1}{2})$, the repeated quantum channel with finite depth is sufficient for the emergence of the SW-SSB in the output state.

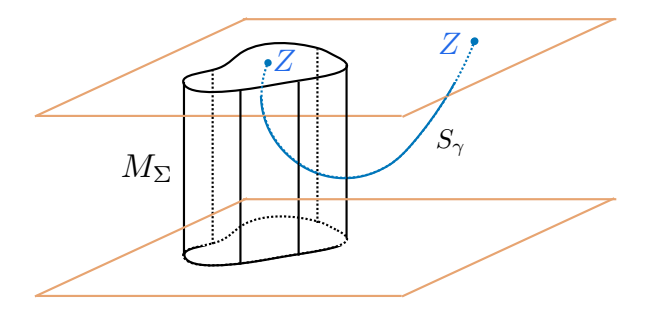


FIG. 13. The existence of the string symmetry operator S_{γ} with γ being any deformable path connecting two points on the top boundary indicates SW-SSB on the top boundary. For a constant but large L_z (the linear size along the z direction), the membrane M_{Σ} will be suppressed, implying the emergence of S_{γ} and therefore, SW-SSB on the top boundary.

First, we notice that at the fixed-point limit $p_z = \frac{1}{2}$, the 3d holographic wavefunction is symmetric under the string operators S_{γ} consisting of a product of Pauli-Zs, with two endpoints attached to the top boundary (see Fig.13). Such a string symmetry operator will be reduced to a weak symmetry $Z_iZ_j\rho Z_iZ_j = \rho$ for the top-boundary reduced density matrix, which indicates a long-range order in the fidelity correlators and SW-SSB.

At $p \neq \frac{1}{2}$, the fixed-point holographic toric code is deformed by $e^{g_z \sum_{\ell \in x-y \text{ plane}} X_\ell}$, and the question is: what is the required depth (namely, the linear size along the z direction) so that S_{γ} can be emergent.

To estimate the depth, one can expand $e^{g_z \sum_{\ell \in x-y \text{ plane}} X_\ell} \propto \prod_{\ell \in x-y \text{ plane}} (1 + \tanh g_z X_\ell)$, so the Pauli-X is applied with a probability amplitude $\tanh g_z$. Since the S_γ string is deformable, in order to modify its expectation values, the application of Pauli-Xs must form a membrane M_Σ extending along the z direction from the top boundary to the bottom boundary, and the membrane Σ must form a closed loop in the x-y plane that encloses one endpoint of S_γ on the top boundary. Such a membrane will necessarily intersect with S_γ for any deformable string γ .

Now we estimate the probability of forming such a membrane M_{Σ} with size L_z along the z direction and a circumference L_{xy} on the x-y plane. First, to form such a membrane of Pauli-Xs, the corresponding probability weight is $(\tanh g_z)^{L_z L_{xy}}$. Meanwhile, the closed loop on the x-y plane is deformable, so one needs to introduce a multiplicity factor $\sim 3^{L_{xy}}$. Therefore, the probability of forming a M_{γ} to intersect with S_{γ} is roughly

$$(\tanh g_z)^{L_z L_{xy}} 3^{L_{xy}} = (3(\tanh g_z)^{L_z})^{L_{xy}}$$
 (C1)

As such, for a large but finite L_z , the probability of forming M_{Σ} decays exponentially with L_{xy} , meaning S_{γ} can be emergent and gives rise to the desired SW-SSB on the top boundary. This argument is in spirit similar to the Peierls' argument for the existence of an ordered phase in 2d Ising model [127].

Appendix D: Holographic bulk of the 2d 0-form SW-SSB

In Sec.V A, we consider the quantum channel $\mathcal{E} = \prod_{i} \mathcal{E}_{i}^{z} \mathcal{E}_{i}^{x}$ (Eq.37), defined as

$$\mathcal{E}_{ij}^{z}[\rho_{0}] = (1 - p_{z})\rho_{0} + p_{z}Z_{i}Z_{j}\rho_{0}Z_{i}Z_{j}.$$

$$\mathcal{E}_{i}^{x}[\rho_{0}] = (1 - p_{x})\rho_{0} + p_{x}X_{i}\rho_{0}X_{i}.$$
(D1)

The steady state of the channel is the SW-SSB density matrix $\rho \propto 1 + \prod_i X_i$. Here, we present the detailed operator mapping to show that the bulk exhibits a 3d toric-code topological order. We will focus on the fixed-point limit $(p_x = p_z = \frac{1}{2})$, and the non-fixed point limit can be easily obtained by applying an imaginary-time deformation, as in Eq.A6.

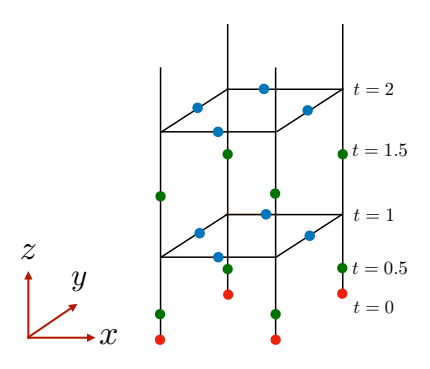


FIG. 14. The input of the repeated quantum channel (Eq.D1) is denoted by the red qubits. They constantly travel upward (along the z direction) to unitarily entangle with the green and blue ancilla qubits. Tracing out the ancilla qubits leads to the output of the quantum channel.

To repeatedly implement the channel, the input red system qubits are constantly moving up to sequentially interact with the green and blue ancilla qubits, which are responsible for the ZZ noise and X noise, as shown in Fig. 14. In particular, the green and blue ancilla qubits are initialized at $|+\rangle$ and $|0\rangle$, respectively. The unitary gate that entangles the ancilla green qubits and the system red qubits is given by

$$u_x = |0\rangle \langle 0|_a + |1\rangle \langle 1|_a X_s. \tag{D2}$$

The unitary gate that entangles the ancilla blue qubits and the system red qubits is given by

$$u_z = |+\rangle \langle +|_a + |-\rangle \langle -|_a Z_s, \tag{D3}$$

Since the green qubits are initialized at $|+\rangle$, the initial state before applying the sequential unitary circuit U has the XX stabilizer on the two neighboring qubits on the z links (Fig.15(a)). One can check that after the conjugation of U, it is mapped to $X^{\otimes 6}$ on the 6 links around a vertex, i.e., the vertex stabilizers of the 3d toric code. On the other hand, since all the ancilla (blue) qubits on the x-y plane are initialized in $|0\rangle$, the initial state has

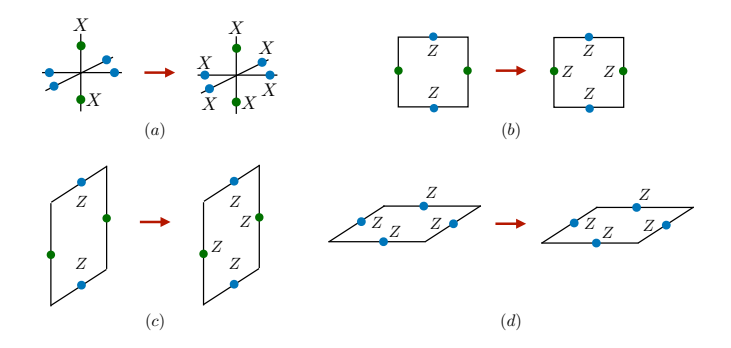


FIG. 15. Operator mapping under the sequential unitary circuit U that implements the repeated application of the channel defined in Eq.D1.

the $Z^{\otimes 2}$ stabilizer on the two links of an x-z plane plaquette (Fig.15(b)). Under the conjugation of U, it is mapped to the plaquette operator $Z^{\otimes 4}$ in the x-z plane. Similarly, the $Z^{\otimes 2}$ stabilizer on the two links of a y-z plane plaquette (Fig.15(c)) is mapped to the plaquette operator $Z^{\otimes 4}$ in the y-z plane. Finally, the initial state of the ancilla qubits also has the plaquette operator $Z^{\otimes 4}$ on the x-y plane (Fig.15(d)), and it is invariant under the sequential unitary circuit U. The existence of these star and plaquette stabilizers therefore indicates a 3d toric-code topological order.

Appendix E: Holographic bulk of the 2d 1-form SW-SSB

In Sec.VB, we consider the following channel $\mathcal{E} = \prod_{v} \mathcal{E}_{v}^{z} \prod_{\ell} \mathcal{E}_{\ell}^{x}$ defined as

$$\mathcal{E}_{\ell}^{x}[\rho] = (1 - p_x)\rho + p_x X_{\ell} \rho X_{\ell}.$$

$$\mathcal{E}_{v}^{z}[\rho] = (1 - p_z)\rho + p_z A_v \rho A_v,$$
 (E1)

where A_v is a $Z^{\otimes 4}$ acting on the four links around a vertex. Given any input state with the strong 1-form symmetry generated by $B_p = \prod_{\ell \in p} X_\ell$, the output state is $\rho \propto \prod_p (1+B_p)$. Here we show that the holographic wavefunction is a 3d toric-code topological order with m-loop condensed boundary.

Specifically, we will focus on the fixed-point limit $p_x = p_z = \frac{1}{2}$, and show the emergence of the fixed-point toric-code stabilizers.

To repeatedly implement the channel, the input red system qubits are constantly moving up to sequentially interact with the green and blue ancilla qubits, which are responsible for the Z-type noise and X-type noise, as shown in Fig. 16.

The blue ancilla qubits live on the links in the x-y plane. They are initialized at $|+\rangle$. The X-type noise can be implemented by entangling a system (red) qubit and a blue qubit via the gate

$$u_x = |0\rangle \langle 0|_a + |1\rangle \langle 1|_a X_s.$$
 (E2)

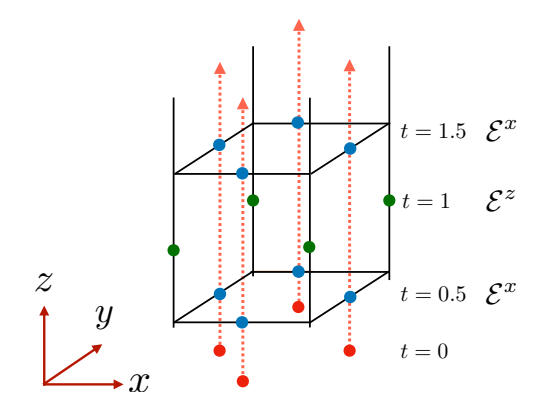


FIG. 16. The input of the repeated quantum channel (Eq.E1) is denoted by the red qubits. They constantly travel upward (along the z direction) to unitarily entangle with the green and blue ancilla qubits. Tracing out the ancilla qubits leads to the output of the quantum channel.

This process can be explained more explicitly through Fig.16: in the time slice when t=0.5, all the red qubits travel to the links on the x-y plane. A single red qubit will entangle with another blue qubit at the same location using the u_x gate.

The green ancilla qubits live on the links oriented along the z direction. They are initialized at $|0\rangle$. The Z-type noise can be implemented by entangling a system (red) qubit and a green qubit via the gate

$$u_z = |+\rangle \langle +|_a + |-\rangle \langle -|_a Z_s.$$
 (E3)

More explicitly, in the time slice when t=1 (Fig.16), all the red qubits travel to the centers of the x-z plane plaquettes and the centers of the y-z plane plaquettes; a single red qubit will entangle with its two neighboring green qubits, both using the u_z gate. Equivalently, a single green qubit will entangle with four green qubits on the four neighboring plaquettes, all using the u_z gate.

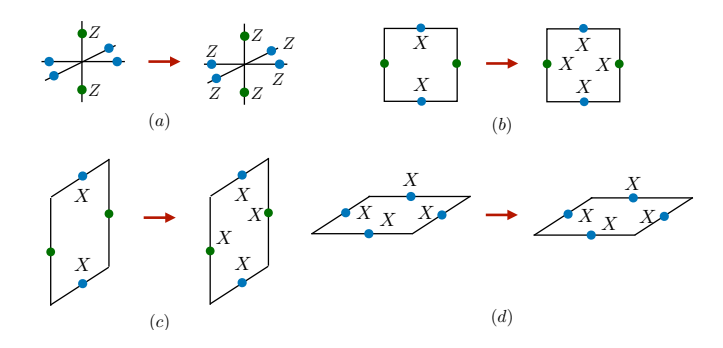


FIG. 17. Operator mapping under the sequential unitary circuit U that implements the repeated application of the channel defined in Eq.E1.

With the application of the sequential unitary circuit, one can derive the operator mapping rules under the circuit conjugation (Fig. 17). The emergence of the star

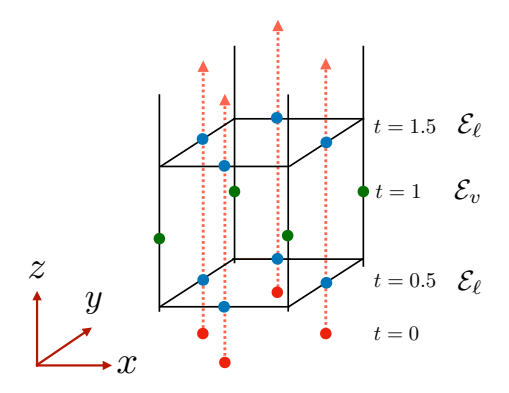


FIG. 18. The input of the repeated quantum channel (Eq.F1) is denoted by the red qubits. They constantly travel upward (along the z direction) to unitarily entangle with the green and blue ancilla qubits. Tracing out the ancilla qubits leads to the output of the quantum channel.

and plaquette stabilizers indicates the 3d toric-code topological order. We note that the operator mapping in (d) requires the red qubits to have the strong 1-form symmetry generated by $B_p = \prod_{\ell \in p} X_{\ell}$. This is because when the red qubits interact with the blue qubits via the onsite u_x gate, the $X^{\otimes 4}$ stabilizer on the blue qubits is, in fact, mapped to a product of $X^{\otimes 4}$ (on the blue qubits) and B_p (on the red qubits). Only when $B_p = 1$, $X^{\otimes 4}$ of the blue qubits can be invariant under the circuit dynamics.

Appendix F: Holographic bulk of the 2d fermionic 1-form SW-SSB

In Sec. VE, we consider the channel $\mathcal{E} = \prod_v \mathcal{E}_v \prod_\ell \mathcal{E}_\ell$ with

$$\begin{split} \mathcal{E}_{\ell}[\rho] &= p_{\ell}\rho + (1 - p_{\ell})X_{\ell}Z_{\ell + \frac{\hat{x}}{2} - \frac{\hat{y}}{2}}\rho X_{\ell}Z_{\ell + \frac{\hat{x}}{2} - \frac{\hat{y}}{2}} \\ \mathcal{E}_{v}[\rho] &= p_{v}\rho + (1 - p_{v})A_{v}\rho A_{v} \end{split} \tag{F1}$$

Here we discuss details regarding the emergence of the 3d holographic wavefunction. We will focus on the fixed-point limit $p_{\ell}=p_v=\frac{1}{2}$, and show the emergence of the fixed-point 3d fermionic toric-code stabilizers.

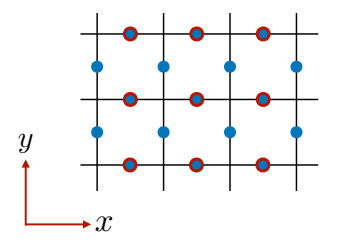
To repeatedly implement the channel, the input red system qubits are constantly moving up to sequentially interact with the blue and green ancilla qubits, which are responsible for the \mathcal{E}_{ℓ} channel and \mathcal{E}_{v} , as shown in Fig. 18.

The blue ancilla qubits live on the links in the x-y plane. They are initialized at $|+\rangle$. \mathcal{E}_{ℓ} can be implemented by entangling a system (red) qubit and a blue qubit via the gate

$$u_{\ell} = |0\rangle \langle 0|_{a,\ell} + |1\rangle \langle 1|_{a,\ell} X_{\ell} Z_{\ell + \frac{x}{2} - \frac{y}{2}}.$$
 (F2)

where $|0\rangle_{a,\ell}$, $|1\rangle_{a,\ell}$ and the state of the blue ancilla qubit at the link ℓ , and $X_\ell Z_{\ell+\frac{x}{2}-\frac{y}{2}}$ is the operator acting on the two system qubits.

This process can be explained more explicitly through Fig.18: in the time slice when t=0.5, all the red qubits travel to the links on the x-y plane and they interact with the blue qubits with $\prod_{\ell} u_{\ell}$. Notice that neighboring u_{ℓ} may not commute, so we would need to specify the time order for the application of the u_{ℓ} gate. Our choice is shown as follows:



We first simultaneously apply u_{ℓ} on all the x-links, and then simultaneously apply u_{ℓ} on all the y-links. While the choice of the order of the gate applied affects the detail of the 3d bulk stabilizers, it does not affect the quantum channel on the system red qubits.

The green ancilla qubits live on the links oriented along the z direction. They are initialized at $|0\rangle$. The Z-type noise can be implemented by entangling a system (red) qubit and a green qubit via the gate

$$u_z = |+\rangle \langle +|_a + |-\rangle \langle -|_a A_v.$$
 (F3)

More explicitly, in the time slice when t=1 (Fig.16), all the red qubits travel to the centers of the x-z plane plaquettes and the centers of the y-z plane plaquettes; a single red qubit will entangle with its two neighboring green qubits, both using the u_z gate. Equivalently, a single green qubit will entangle with four green qubits on the four neighboring plaquettes, all using the u_z gate.

With the application of the sequential unitary circuit, one can then derive the operator mapping rules under the circuit conjugation, shown in Fig. 19.

^[1] X.-G. Wen, Quantum field theory of many-body systems: From the origin of sound to an origin of light and electrons (Oxford university press, 2004).

^[2] M. B. Hastings and X.-G. Wen, Quasiadiabatic con-

tinuation of quantum states: The stability of topological ground-state degeneracy and emergent gauge invariance, Phys. Rev. B **72**, 045141 (2005).

^[3] X. Chen, Z.-C. Gu, and X.-G. Wen, Local unitary trans-

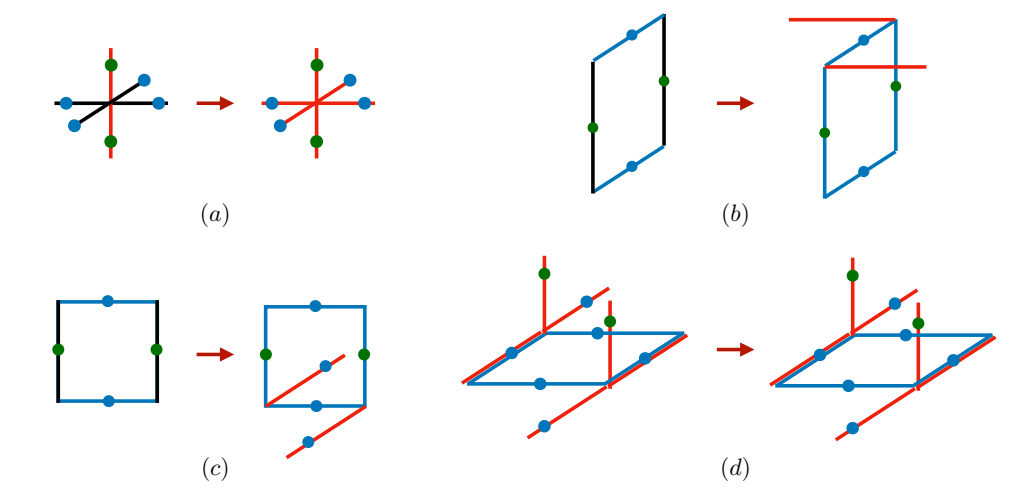


FIG. 19. Operator mapping under the sequential unitary circuit that implements the repeated application of the channel defined in Eq.F1. The red and blue links denote the Pauli-X and Pauli-Z, respectively; no Pauli operators are supported on black links.

- formation, long-range quantum entanglement, wave function renormalization, and topological order, Phys. Rev. B 82, 155138 (2010).
- [4] X. Chen, Z.-C. Gu, and X.-G. Wen, Classification of gapped symmetric phases in one-dimensional spin systems, Phys. Rev. B 83, 035107 (2011).
- [5] X. Chen, Z.-C. Gu, and X.-G. Wen, Complete classification of one-dimensional gapped quantum phases in interacting spin systems, Phys. Rev. B 84, 235128 (2011).
- [6] E. Dennis, A. Kitaev, A. Landahl, and J. Preskill, Topological quantum memory, Journal of Mathematical Physics 43, 4452–4505 (2002).
- [7] R. Fan, Y. Bao, E. Altman, and A. Vishwanath, Diagnostics of mixed-state topological order and breakdown of quantum memory, PRX Quantum 5, 020343 (2024).
- [8] C. de Groot, A. Turzillo, and N. Schuch, Symmetry Protected Topological Order in Open Quantum Systems, Quantum 6, 856 (2022).
- [9] J. Y. Lee, Y.-Z. You, and C. Xu, Symmetry protected topological phases under decoherence, Quantum 9, 1607 (2025).
- [10] J. Y. Lee, Exact calculations of coherent information for toric codes under decoherence: Identifying the fundamental error threshold, Phys. Rev. Lett. 134, 250601 (2025).
- [11] R. Niwa and J. Y. Lee, Coherent information for calderbank-shor-steane codes under decoherence, Phys. Rev. A 111, 032402 (2025).
- [12] R. Ma and C. Wang, Average symmetry-protected topological phases, Phys. Rev. X 13, 031016 (2023).
- [13] R. Ma, J.-H. Zhang, Z. Bi, M. Cheng, and C. Wang, Topological phases with average symmetries: The decohered, the disordered, and the intrinsic, Phys. Rev. X 15, 021062 (2025).
- [14] J.-H. Zhang, K. Ding, S. Yang, and Z. Bi, Fractonic higher-order topological phases in open quantum systems, Phys. Rev. B 108, 155123 (2023).
- [15] R. Ma and A. Turzillo, Symmetry-protected topological phases of mixed states in the doubled space, PRX Quantum 6, 010348 (2025).
- [16] H. Xue, J. Y. Lee, and Y. Bao, Tensor network formula-

- tion of symmetry protected topological phases in mixed states, arXiv preprint arXiv:2403.17069 (2024).
- [17] Y. Guo, J.-H. Zhang, H.-R. Zhang, S. Yang, and Z. Bi, Locally purified density operators for symmetryprotected topological phases in mixed states, Phys. Rev. X 15, 021060 (2025).
- [18] Y.-H. Chen and T. Grover, Separability transitions in topological states induced by local decoherence, Phys. Rev. Lett. 132, 170602 (2024).
- [19] Y.-H. Chen and T. Grover, Unconventional topological mixed-state transition and critical phase induced by self-dual coherent errors, Phys. Rev. B 110, 125152 (2024).
- [20] Y.-H. Chen and T. Grover, Symmetry-enforced manybody separability transitions, PRX Quantum 5, 030310 (2024).
- [21] L. A. Lessa, M. Cheng, and C. Wang, Mixed-state quantum anomaly and multipartite entanglement, Phys. Rev. X 15, 011069 (2025).
- [22] Z. Wang and L. Li, Anomaly in open quantum systems and its implications on mixed-state quantum phases, PRX Quantum 6, 010347 (2025).
- [23] T. D. Ellison and M. Cheng, Toward a classification of mixed-state topological orders in two dimensions, PRX Quantum 6, 010315 (2025).
- [24] R. Sohal and A. Prem, Noisy approach to intrinsically mixed-state topological order, PRX Quantum 6, 010313 (2025).
- [25] T.-C. Lu, Z. Zhang, S. Vijay, and T. H. Hsieh, Mixed-state long-range order and criticality from measurement and feedback, PRX Quantum 4, 030318 (2023).
- [26] T.-C. Lu, T. H. Hsieh, and T. Grover, Detecting topological order at finite temperature using entanglement negativity, Phys. Rev. Lett. 125, 116801 (2020).
- [27] S. Chirame, F. J. Burnell, S. Gopalakrishnan, and A. Prem, Stable symmetry-protected topological phases in systems with heralded noise, Phys. Rev. Lett. 134, 010403 (2025).
- [28] V. V. Albert and L. Jiang, Symmetries and conserved quantities in lindblad master equations, Phys. Rev. A 89, 022118 (2014).

- [29] C. Zhang, Y. Xu, J.-H. Zhang, C. Xu, Z. Bi, and Z.-X. Luo, Strong-to-weak spontaneous breaking of 1form symmetry and intrinsically mixed topological order, Phys. Rev. B 111, 115137 (2025).
- [30] J.-H. Zhang, C. Xu, and Y. Xu, Fluctuation-dissipation theorem and information geometry in open quantum systems, arXiv preprint arXiv:2409.18944 (2024).
- [31] R. Raussendorf, J. Harrington, and K. Goyal, Topological fault-tolerance in cluster state quantum computation, New Journal of Physics 9, 199 (2007).
- [32] F. Eckstein, B. Han, S. Trebst, and G.-Y. Zhu, Robust teleportation of a surface code and cascade of topological quantum phase transitions, PRX Quantum 5, 040313 (2024).
- [33] J. Y. Lee, W. Ji, Z. Bi, and M. P. A. Fisher, Decoding measurement-prepared quantum phases and transitions: from ising model to gauge theory, and beyond (2022), arXiv:2208.11699 [cond-mat.str-el].
- [34] G.-Y. Zhu, N. Tantivasadakarn, A. Vishwanath, S. Trebst, and R. Verresen, Nishimori's cat: Stable long-range entanglement from finite-depth unitaries and weak measurements, Phys. Rev. Lett. 131, 200201 (2023).
- [35] F. Fang, K. Wang, V. S. Liu, Y. Wang, R. Cimmino, J. Wei, M. Bintz, A. Parr, J. Kemp, K.-K. Ni, and N. Y. Yao, Probing critical phenomena in open quantum systems using atom arrays (2024), arXiv:2402.15376 [quant-ph].
- [36] A. Coser and D. Pérez-García, Classification of phases for mixed states via fast dissipative evolution, Quantum 3, 174 (2019).
- [37] Y. Bao, R. Fan, A. Vishwanath, and E. Altman, Mixed-state topological order and the errorfield double formulation of decoherence-induced transitions, arXiv preprint arXiv:2301.05687 (2023).
- [38] S. Sang, Y. Zou, and T. H. Hsieh, Mixed-state quantum phases: Renormalization and quantum error correction, Phys. Rev. X 14, 031044 (2024).
- [39] J.-H. Zhang, Y. Qi, and Z. Bi, Strange correlation function for average symmetry-protected topological phases, arXiv preprint arXiv:2210.17485 (2022).
- [40] B. J. Brown, D. Loss, J. K. Pachos, C. N. Self, and J. R. Wootton, Quantum memories at finite temperature, Rev. Mod. Phys. 88, 045005 (2016).
- [41] Z. Wang, Z. Wu, and Z. Wang, Intrinsic mixed-state topological order, PRX Quantum 6, 010314 (2025).
- [42] A. Antinucci, G. Galati, G. Rizi, and M. Serone, Symmetries and topological operators, on average, SciPost Phys. 15, 125 (2023).
- [43] T.-C. Lu and S. Vijay, Characterizing long-range entanglement in a mixed state through an emergent order on the entangling surface, Phys. Rev. Res. 5, 033031 (2023).
- [44] Y. You and M. Oshikawa, Intrinsic symmetry-protected topological mixed state from modulated symmetries and hierarchical structure of boundary anomaly, Phys. Rev. B 110, 165160 (2024).
- [45] T.-C. Lu, Disentangling transitions in topological order induced by boundary decoherence, Phys. Rev. B 110, 125145 (2024).
- [46] T.-C. Lu, S. Gopalakrishnan, and Y. You, Spacetime duality between sequential and measurement-feedback circuits, arXiv preprint arXiv:2507.12523 (2025).
- [47] K. Su, N. Myerson-Jain, C. Wang, C.-M. Jian, and

- C. Xu, Higher-form symmetries under weak measurement, Phys. Rev. Lett. **132**, 200402 (2024).
- [48] L. A. Lessa, S. Sang, T.-C. Lu, T. H. Hsieh, and C. Wang, Higher-form anomaly and longrange entanglement of mixed states, arXiv preprint arXiv:2503.12792 (2025).
- [49] S. Sang and T. H. Hsieh, Stability of mixed-state quantum phases via finite markov length, Phys. Rev. Lett. 134, 070403 (2025).
- [50] A. Moharramipour, L. A. Lessa, C. Wang, T. H. Hsieh, and S. Sahu, Symmetry-enforced entanglement in maximally mixed states, PRX Quantum 5, 040336 (2024).
- [51] S. Sang, T. H. Hsieh, and Y. Zou, Approximate quantum error correcting codes from conformal field theory, Phys. Rev. Lett. 133, 210601 (2024).
- [52] Y. Guo, K. Ding, and S. Yang, A new framework for quantum phases in open systems: Steady state of imaginary-time lindbladian evolution (2024), arXiv:2408.03239 [quant-ph].
- [53] D. Gu, Z. Wang, and Z. Wang, Spontaneous symmetry breaking in open quantum systems: strong, weak, and strong-to-weak, arXiv preprint arXiv:2406.19381 (2024).
- [54] J. Y. Lee, C.-M. Jian, and C. Xu, Quantum criticality under decoherence or weak measurement, PRX Quantum 4, 030317 (2023).
- [55] P. Sala, S. Gopalakrishnan, M. Oshikawa, and Y. You, Spontaneous strong symmetry breaking in open systems: Purification perspective, Phys. Rev. B 110, 155150 (2024).
- [56] L. A. Lessa, R. Ma, J.-H. Zhang, Z. Bi, M. Cheng, and C. Wang, Strong-to-weak spontaneous symmetry breaking in mixed quantum states, PRX Quantum 6, 010344 (2025).
- [57] Z. Song and J.-H. Zhang, Strong-to-weak spontaneous symmetry breaking of higher-form non-invertible symmetries in kitaev's quantum double model, arXiv preprint arXiv:2509.24179 (2025).
- [58] X. Huang, M. Qi, J.-H. Zhang, and A. Lucas, Hydrodynamics as the effective field theory of strong-to-weak spontaneous symmetry breaking, Phys. Rev. B 111, 125147 (2025).
- [59] P. Sala, F. Pollmann, M. Oshikawa, and Y. You, Entanglement holography in quantum phases via twisted r\'enyi-n correlators, arXiv preprint arXiv:2506.10076 (2025).
- [60] C. Zhang, Y. Xu, J.-H. Zhang, C. Xu, Z. Bi, and Z.-X. Luo, Strong-to-weak spontaneous breaking of 1form symmetry and intrinsically mixed topological order, Phys. Rev. B 111, 115137 (2025).
- [61] Y.-J. Liu and S. Lieu, Dissipative phase transitions and passive error correction, Phys. Rev. A 109, 022422 (2024).
- [62] X. Feng, Z. Cheng, and M. Ippoliti, Hardness of observing strong-to-weak symmetry breaking, Physical Review Letters 135, 200402 (2025).
- [63] J. McGreevy, Generalized symmetries in condensed matter, Annual Review of Condensed Matter Physics 14, 57 (2023).
- [64] J. Kim, E. Altman, and J. Y. Lee, Error threshold of syk codes from strong-to-weak parity symmetry breaking, arXiv preprint arXiv:2410.24225 (2024).
- [65] Z. Wang, X.-D. Dai, H.-R. Wang, and Z. Wang, Topologically ordered steady states in open quantum sys-

- tems, SciPost Phys. 17, 167 (2024).
- [66] X.-D. Dai, Z. Wang, H.-R. Wang, and Z. Wang, Steadystate topological order, Physical Review B 111, 115142 (2025).
- [67] B. Aldossari, S. Blinov, and Z.-X. Luo, Tensor network representations for intrinsically mixed-state topological orders, arXiv preprint arXiv:2507.22989 (2025).
- [68] T.-H. Yang, B. Shi, and J. Y. Lee, Topological mixed states: Axiomatic approaches and phases of matter, arXiv preprint arXiv:2506.04221 (2025).
- [69] S. Sang, L. A. Lessa, R. S. Mong, T. Grover, C. Wang, and T. H. Hsieh, Mixed-state phases from local reversibility, arXiv preprint arXiv:2507.02292 (2025).
- [70] Y. Liu, A. Ruiz-de Alarcón, G. Styliaris, X.-Q. Sun, D. Pérez-García, and J. I. Cirac, Parent lindbladians for matrix product density operators, arXiv preprint arXiv:2501.10552 (2025).
- [71] N. Ziereis, S. Moudgalya, and M. Knap, Strong-to-weak symmetry breaking phases in steady states of quantum operations, arXiv preprint arXiv:2509.09669 (2025).
- [72] T. Rakovszky, S. Gopalakrishnan, and C. von Keyserlingk, Defining stable phases of open quantum systems, Phys. Rev. X 14, 041031 (2024).
- [73] X. Chen, M. Hermele, and D. T. Stephen, Sequential adiabatic generation of chiral topological states, arXiv preprint arXiv:2402.03433 (2024).
- [74] X. Chen, A. Dua, M. Hermele, D. T. Stephen, N. Tantivasadakarn, R. Vanhove, and J.-Y. Zhao, Sequential quantum circuits as maps between gapped phases, Physical Review B 109, 075116 (2024).
- [75] M. P. Zaletel and F. Pollmann, Isometric tensor network states in two dimensions, Phys. Rev. Lett. 124, 037201 (2020).
- [76] S. Gopalakrishnan, Push-down automata as sequential generators of highly entangled states, Journal of Physics A: Mathematical and Theoretical 58, 055301 (2025).
- [77] S. Sun, J.-H. Zhang, Z. Bi, and Y. You, Holographic view of mixed-state symmetry-protected topological phases in open quantum systems, PRX Quantum 6, 020333 (2025).
- [78] T. Soejima, K. Siva, N. Bultinck, S. Chatterjee, F. Pollmann, and M. P. Zaletel, Isometric tensor network representation of string-net liquids, Phys. Rev. B 101, 085117 (2020).
- [79] Y.-J. Liu, K. Shtengel, A. Smith, and F. Pollmann, Methods for simulating string-net states and anyons on a digital quantum computer, PRX Quantum 3, 040315 (2022).
- [80] R. Luo, Y.-N. Wang, and Z. Bi, Topological holography for mixed-state phases and phase transitions, arXiv preprint arXiv:2507.06218 (2025).
- [81] M. Qi, R. Sohal, X. Chen, D. T. Stephen, and A. Prem, The symmetry taco: Equivalences between gapped, gapless, and mixed-state spts, arXiv preprint arXiv:2507.05335 (2025).
- [82] S. Schafer-Nameki, A. Tiwari, A. Warman, and C. Zhang, Symtft approach for mixed states with noninvertible symmetries, arXiv preprint arXiv:2507.05350 (2025).
- [83] M. Levin and X.-G. Wen, Detecting topological order in a ground state wave function, Phys. Rev. Lett. 96, 110405 (2006).
- [84] A. Kitaev and J. Preskill, Topological entanglement entropy, Phys. Rev. Lett. 96, 110404 (2006).

- [85] S. Papanikolaou, K. S. Raman, and E. Fradkin, Topological phases and topological entropy of twodimensional systems with finite correlation length, Phys. Rev. B 76, 224421 (2007).
- [86] C. Castelnovo and C. Chamon, Quantum topological phase transition at the microscopic level, Phys. Rev. B 77, 054433 (2008).
- [87] Y. Xu and C.-M. Jian, Average-exact mixed anomalies and compatible phases, Phys. Rev. B 111, 125128 (2025).
- [88] Y.-J. Liu, W.-T. Xu, F. Pollmann, and M. Knap, Detecting emergent 1-form symmetries with quantum error correction, arXiv:2502.17572 (2025).
- [89] L. Kong, T. Lan, X.-G. Wen, Z.-H. Zhang, and H. Zheng, Algebraic higher symmetry and categorical symmetry: A holographic and entanglement view of symmetry, Phys. Rev. Res. 2, 043086 (2020).
- [90] A. Chatterjee and X.-G. Wen, Symmetry as a shadow of topological order and a derivation of topological holographic principle, Phys. Rev. B 107, 155136 (2023).
- [91] S. D. Pace and X.-G. Wen, Exact emergent higher-form symmetries in bosonic lattice models, Phys. Rev. B 108, 195147 (2023).
- [92] I. H. Kim, M. Levin, T.-C. Lin, D. Ranard, and B. Shi, Universal lower bound on topological entanglement entropy, Phys. Rev. Lett. 131, 166601 (2023).
- [93] M. Levin, Physical proof of the topological entanglement entropy inequality, Phys. Rev. B 110, 165154 (2024).
- [94] A. Uhlmann, The "transition probability" in the state space of a*-algebra, Reports on Mathematical Physics 9, 273 (1976).
- [95] Y.-J. Liu, K. Shtengel, and F. Pollmann, Simulating two-dimensional topological quantum phase transitions on a digital quantum computer, Phys. Rev. Res. 6, 043256 (2024).
- [96] J. Boesl, Y.-J. Liu, W.-T. Xu, F. Pollmann, and M. Knap, Quantum phase transitions between symmetry-enriched fracton phases, Phys. Rev. B 112, 125152 (2025).
- [97] J. Boesl, Y.-J. Liu, F. Pollmann, and M. Knap, Skeleton of isometric tensor network states for abelian string-net models, arXiv:2511.13821 (2025).
- [98] N. Schuch, I. Cirac, and D. Pérez-García, Peps as ground states: Degeneracy and topology, Annals of Physics 325, 2153 (2010).
- [99] D. J. Williamson, N. Bultinck, M. Mariën, M. B. Şahinoğlu, J. Haegeman, and F. Verstraete, Matrix product operators for symmetry-protected topological phases: Gauging and edge theories, Phys. Rev. B 94, 205150 (2016).
- [100] M. B. Şahinoğlu, D. Williamson, N. Bultinck, M. Mariën, J. Haegeman, N. Schuch, and F. Verstraete, Characterizing topological order with matrix product operators, Annales Henri Poincaré 22, 563 (2021).
- [101] N. Bultinck, M. Mariën, D. Williamson, M. Şahinoğlu, J. Haegeman, and F. Verstraete, Anyons and matrix product operator algebras, Annals of Physics 378, 183 (2017).
- [102] J. I. Cirac, D. Poilblanc, N. Schuch, and F. Verstraete, Entanglement spectrum and boundary theories with projected entangled-pair states, Phys. Rev. B 83, 245134 (2011).
- [103] J. Cirac, D. Pérez-García, N. Schuch, and F. Ver-

- straete, Matrix product density operators: Renormalization fixed points and boundary theories, Annals of Physics 378, 100 (2017).
- [104] A. Molnar, A. R. de Alarcón, J. Garre-Rubio, N. Schuch, J. I. Cirac, and D. Pérez-García, Matrix product operator algebras i: representations of weak hopf algebras and projected entangled pair states, arXiv preprint arXiv:2204.05940 (2022).
- [105] R. J. Baxter, Exactly solved models in statistical mechanics (1982).
- [106] W. Shirley, K. Slagle, and X. Chen, Fractional excitations in foliated fracton phases, Annals of Physics 410, 167922 (2019).
- [107] Y. You and F. von Oppen, Majorana quantum lego, a route towards fracton matter, arXiv preprint arXiv:1812.06091 (2018).
- [108] M. Levin and X.-G. Wen, Fermions, strings, and gauge fields in lattice spin models, Phys. Rev. B 67, 245316 (2003).
- [109] C. W. von Keyserlingk and F. J. Burnell, Walker-wang models and axion electrodynamics, Phys. Rev. B 91, 045134 (2015).
- [110] Y.-A. Chen and A. Kapustin, Bosonization in three spatial dimensions and a 2-form gauge theory, Phys. Rev. B 100, 245127 (2019).
- [111] Y.-A. Chen, T. D. Ellison, and N. Tantivasadakarn, Disentangling supercohomology symmetry-protected topological phases in three spatial dimensions, Phys. Rev. Res. 3, 013056 (2021).
- [112] S.-T. Zhou, M. Cheng, T. Rakovszky, C. von Keyserlingk, and T. D. Ellison, Finite-temperature quantum topological order in three dimensions, Phys. Rev. Lett. 135, 040402 (2025).
- [113] J. Hauser, Y. Bao, S. Sang, A. Lavasani, U. Agrawal, and M. Fisher, Information dynamics in decohered quantum memory with repeated syndrome measurements: A dual approach, arXiv preprint arXiv:2407.07882 (2024).
- [114] Q. Wang, R. Vasseur, S. Trebst, A. W. Ludwig, and G.-Y. Zhu, Decoherence-induced self-dual criticality in topological states of matter, arXiv preprint

- arXiv:2502.14034 (2025).
- [115] A.-R. Negari, T. D. Ellison, and T. H. Hsieh, Spacetime markov length: a diagnostic for fault tolerance via mixed-state phases, arXiv preprint arXiv:2412.00193 (2024).
- [116] M.-Y. Li and P. Ye, Subdimensional entanglement entropy: from virtual response to mixed-state holography, arXiv preprint arXiv:2510.15766 (2025).
- [117] X. Huang, M. Qi, J.-H. Zhang, and A. Lucas, Hydrodynamics as the effective field theory of strong-to-weak spontaneous symmetry breaking (2024), arXiv:2407.08760 [cond-mat.str-el].
- [118] K. Su, A. Sarma, M. Bintz, T. Kiely, Y. Bao, M. P. Fisher, and C. Xu, Spin liquid and superconductivity emerging from steady states and measurements, Physical Review Letters 135, 050403 (2025).
- [119] Y. Li, F. Pollmann, N. Read, and P. Sala, Highly entangled stationary states from strong symmetries, Phys. Rev. X 15, 011068 (2025).
- [120] C. H. Bennett, D. P. DiVincenzo, J. A. Smolin, and W. K. Wootters, Mixed-state entanglement and quantum error correction, Phys. Rev. A 54, 3824 (1996).
- [121] A. Peres, Separability criterion for density matrices, Phys. Rev. Lett. 77, 1413 (1996).
- [122] M. Horodecki, P. Horodecki, and R. Horodecki, Separability of mixed states: necessary and sufficient conditions, Physics Letters A 223, 1 (1996).
- [123] J. Eisert and M. B. Plenio, A comparison of entanglement measures, Journal of Modern Optics 46, 145 (1999).
- [124] G. Vidal and R. F. Werner, Computable measure of entanglement, Phys. Rev. A 65, 032314 (2002).
- [125] R. Fan, Y. Wu, Y. Bao, and Z. Dai, No-go theorems for sequential preparation of two-dimensional chiral states via channel-state correspondence, to appear (2025).
- [126] A. Vijav and J. Y. Lee, to appear (2025).
- [127] R. Peierls, On ising's model of ferromagnetism, in Mathematical Proceedings of the Cambridge Philosophical Society, Vol. 32 (Cambridge University Press, 1936) pp. 477–481.